ELSEVIER

Contents lists available at ScienceDirect

Deep-Sea Research Part I

journal homepage: www.elsevier.com/locate/dsri



Detection and characterisation of deep-sea benthopelagic animals from an autonomous underwater vehicle with a multibeam echosounder: A proof of concept and description of data-processing methods



Katherine M. Dunlop^{a,c}, Toby Jarvis^{b,*}, Kelly J. Benoit-Bird^a, Chad M. Waluk^a, David W. Caress^a, Hans Thomas^a, Kenneth L. Smith Jr^a

- ^a Monterey Bay Aquarium Research Institute, 7700 Sandholdt Road, Moss Landing, CA 93940, USA
- ^b Echoview Software Pty Ltd, GPO Box 1387, Hobart, Tasmania 7001, Australia
- ^c Akvaplan-niva, Fram Centre, Hjalmar Johansens Gate 14, 9007 Tromsø, Norway

ARTICLE INFO

Keywords: Deep sea Benthopelagic animals Autonomous underwater vehicle (AUV) Multibeam echosounder (MBES) Echosounder data processing Avoidance behaviour

ABSTRACT

Benthopelagic animals are an important component of the deep-sea ecosystem, yet are notoriously difficult to study, Multibeam echosounders (MBES) deployed on autonomous underwater vehicles (AUVs) represent a promising technology for monitoring this elusive fauna at relatively high spatial and temporal resolution. However, application of this remote-sensing technology to the study of small (relative to the sampling resolution), dispersed and mobile animals at depth does not come without significant challenges with respect to data collection, data processing and vessel avoidance. As a proof of concept, we used data from a downward-looking RESON SeaBat 7125 MBES mounted on a Dorado-class AUV to detect and characterise the location and movement of backscattering targets (which were likely to have been individual fish or squid) within 50 m of the seafloor at ~800 m depth in Monterey Bay, California. The targets were detected and tracked, enabling their numerical density and movement to be characterised. The results revealed a consistent movement of targets downwards away from the AUV that we interpreted as an avoidance response. The large volume and complexity of the data presented a computational challenge, while reverberation and noise, spatial confounding and a marginal sampling resolution relative to the size of the targets caused difficulties for reliable and comprehensive target detection and tracking. Nevertheless, the results demonstrate that an AUV-mounted MBES has the potential to provide unique and detailed information on the in situ abundance, distribution, size and behaviour of both individual and aggregated deep-sea benthopelagic animals. We provide detailed data-processing information for those interested in working with MBES water-column data, and a critical appraisal of the data in the context of aquatic ecosystem research. We consider future directions for deep-sea water-column echosounding, and reinforce the importance of measures to mitigate vessel avoidance in studies of aquatic ecosystems.

1. Introduction

The deep sea is Earth's largest ecosystem. An understanding of deep-sea ecology underpins our ability to sustainably manage this fragile ecosystem and to quantify its critical role in the biogeochemical cycling of carbon and nitrogen (e.g. Koslow et al., 2000; Smith et al., 2009), yet we still know relatively little about key ecological parameters such as animal abundance, distribution, size, behaviour and trophic interaction (Webb et al., 2010; Danovaro et al., 2014). Benthopelagic animals are those that spend at least some of their time in the layer of water just above the bottom (the benthic boundary layer, BBL; McCave, 1976). In

the deep sea, the BBL can extend for 100 m or so above the bottom and is of particular interest due to its elevated biomass and biodiversity compared to the water above (Angel and Boxshall, 1990; Robison, 2004). Deep-sea benthopelagic animals include medusae, holothurians, cephalopods, copepods, decapods and fish (e.g. Wishner, 1980; Smith, 1982; Herring, 2001). They are known to contribute to the flow of carbon through the ecosystem (Smith, 1992) but are elusive due to the logistical difficulties of sampling at depth (e.g. Bailey et al., 2005; Drazen and Seibel, 2007). The various constraints imposed by the deep-sea environment are such that individuals tend to move slowly (Robison, 2004) and are dispersed (e.g. fish generally predate or

E-mail address: toby.jarvis@echoview.com (T. Jarvis).

^{*} Corresponding author.

scavenge as solitary individuals; Gage and Tyler, 1991; Koslow et al., 2000). Some species do form aggregations of varying sizes and densities, but these are unlikely to reach the proportions of their shallowerwater counterparts. Deep-sea benthopelagic animals may range in body size from millimeter scale (e.g. 0.6 mm for calanoid copepods in the Gulf of California; Wiebe et al., 1988) to meter scale (e.g. 6.4 m for Greenland sharks in the Arctic Ocean; MacNeil et al., 2012), and the relationship between size and depth appears to vary with species and location (Stefanescu et al., 1992; Collins et al., 2005).

To date, the primary tools for studying the deep-sea BBL have been trawls, submersibles (human occupied vehicles, HOVs), remotely operated vehicles (ROVs), camera sleds and baited landers (Robison, 2004), each of which have their limitations (Raymond, 2008). Active sonars (echosounders) mounted on autonomous underwater vehicles (AUVs) represent a promising technology for addressing some of these limitations. Echosounders are widely used in freshwater and marine environments to study aquatic animals because they offer the ability to non-invasively monitor large volumes of water at high spatial and temporal resolution (Rudstam et al., 2012; Benoit-Bird and Lawson, 2016). They are therefore valuable tools to consider for deep-sea applications but, despite a number of studies to date (e.g. Smith et al., 1989, 1992; Kloser, 1996; Smith and Baldwin, 1997; Urmy et al., 2012), have yet to gain widespread use in this environment. AUVs are being increasingly used as platforms for echosounders (e.g. Fernandes et al., 2003; Moline et al., 2015), in large part because they can carry these range-limited instruments closer to the targets of interest (e.g. Benoit-Bird et al., 2017). The fact that AUVs rarely use lights and are generally very quiet should help to minimise observer bias associated with animal avoidance or attraction (Griffiths et al., 2001; Clarke et al., 2010), but this question has received limited research attention in the deep sea.

Broadly speaking there are two types of echosounder: single-beam echosounders (SBES) and multibeam echosounders (MBES). The main benefit of an MBES over an SBES is that it can measure a much larger volume of water while maintaining the same or (typically) better sampling resolution (Gerlotto et al., 1999). MBES technology became available for non-military seafloor depth mapping (hydrography) in the 1970s (Renard and Allenou, 1979), and has since been adapted for habitat mapping (Brown and Blondel, 2009) and the detection and characterisation of water-column backscattering targets such as marine mammals, diving birds, fish, zooplankton, suspended sediment and gas bubbles (e.g. Axelsen et al., 2001; Andersen et al., 2006; Benoit-Bird and Au, 2009; Cox et al., 2009; Simmons et al., 2009; Weber et al., 2012; Hightower et al., 2013; Melvin and Cochrane, 2014; Vatnehol, 2016). MBES water-column measurements are also proving useful in characterising the full extent of objects on the bottom such as wrecks that may otherwise have been missed during a traditional hydrographic survey (e.g. Hughes Clarke et al., 2006).

In this paper we describe a proof of concept regarding the ability of an AUV-mounted MBES to detect and characterise deep-sea benthope-lagic animals, and we examine whether the presence of the AUV influenced their behaviour. We provide detailed data-processing information for those interested in working with MBES water-column data, and a critical appraisal of the data to stimulate ideas for the ongoing use of echosounders for deep-sea water-column research.

2. Materials and methods

2.1. AUV setup and deployment

The *D. Allan B.* is a 0.5 m-diameter, 5.2 m-long Dorado-class AUV designed and built by Monterey Bay Aquarium Research Institute (MBARI) for high-resolution seafloor mapping at depths of up to 6000 m (Caress et al., 2008). Of the payload described in Caress et al. (2008), the instruments in operation on the AUV during this survey were the 200/400 kHz SeaBat 7125-AUV MBES (Teledyne RESON, Denmark), the 19/27 kHz ultra-short baseline (USBL) sonar beacon

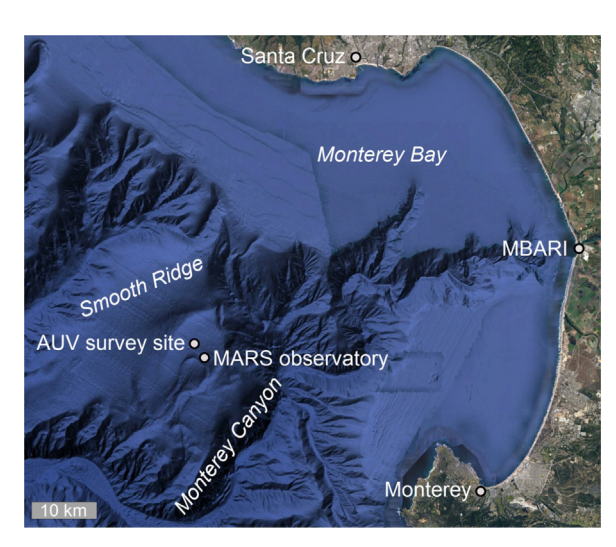


Fig. 1. The locations of MBARI, Smooth Ridge, the MARS observatory and the AUV survey site in Monterey Bay, California. See Section 2.1 for details.

(Sonardyne, UK), the 8–15 kHz acoustic modem (Teledyne Benthos, USA), the Seadevil inertial navigation system (INS; Kearfott, USA), the 300 kHz Doppler velocity log (DVL; Teledyne RD Instruments, USA), the Digiquartz pressure sensor (Paroscientific, USA) and the SBE 49 FastCAT conductivity/temperature/depth (CTD) sensor (Sea-Bird Scientific, USA).

The AUV was deployed from RV *Rachel Carson* at Smooth Ridge in Monterey Bay, California (Fig. 1) on 7th November 2012 to a depth of $\sim\!800\,\mathrm{m}$ ($\sim\!50\,\mathrm{m}$ above the seafloor). Smooth Ridge is a gentle sloping flank covered in sand and sandy mud on the continental slope north of Monterey Canyon, and the AUV survey site was located approximately 4 km from the Monterey Accelerated Research System (MARS) observatory (http://www.mbari.org/at-sea/cabled-observatory). The AUV made multiple repeats of a square survey track of side length $\sim\!200\,\mathrm{m}$, moving at $\sim\!1\,\mathrm{m}$ s $^{-1}$ in a clockwise direction and covering a total distance over ground of $\sim\!47\,\mathrm{km}$ within the coordinates $36.724\!-\!36.727^\circ\mathrm{N}$ and $122.197\!-\!122.199^\circ\mathrm{W}$ (Fig. 2).

2.2. MBES data collection

The SeaBat 7125 (RESON, 2011) is a 2D "swath" MBES capable of recording high-resolution samples of backscattered acoustic pressure (as voltage) that can be used for both water-column and bottom studies (e.g. Weber et al., 2009; Galparsoro et al., 2015). On this deployment the MBES projector and hydrophone were oriented downwards and the system was configured to calculate 256 equiangular sound beams at ~400 kHz (nominally 1° along-track by 0.5° across-track per beam), resulting in a 1° along-track by 128.1° across-track fan (swath) for each narrowband transmission (aka ping or pulse) (Table 1). The MBES and the DVL pinged simultaneously at a rate of 3 pings s⁻¹. RESON 6046 Payload Controller software (Teledyne RESON, Denmark) installed on the AUV's main vehicle computer was used to control the MBES and to record data in the RESON 7k binary data format (s7k files; RESON, 2016). The s7k "record types" of relevance here are record 7000 ("7k Sonar Settings"), record 7004 ("7k Beam Geometry") and record 7018 ("7k Beamformed Data") (see Eq. (1) and Table 1). The GPS, pitch, roll and heading measurements made by the INS were recorded separately in a comma-separated values (csv) file. The accuracy of the nominal environment and MBES-system properties (see Table 1) was not evaluated for this study. The relationship between the raw receiver measurements (see Section 2.3.1) and the acoustic pressure in front of the hydrophone is understood to be complex and potentially non-linear, and the manufacturer recommends that the SeaBat 7125 is not used for quantitative applications (Gorm Wendelboe, pers. comm.). However,

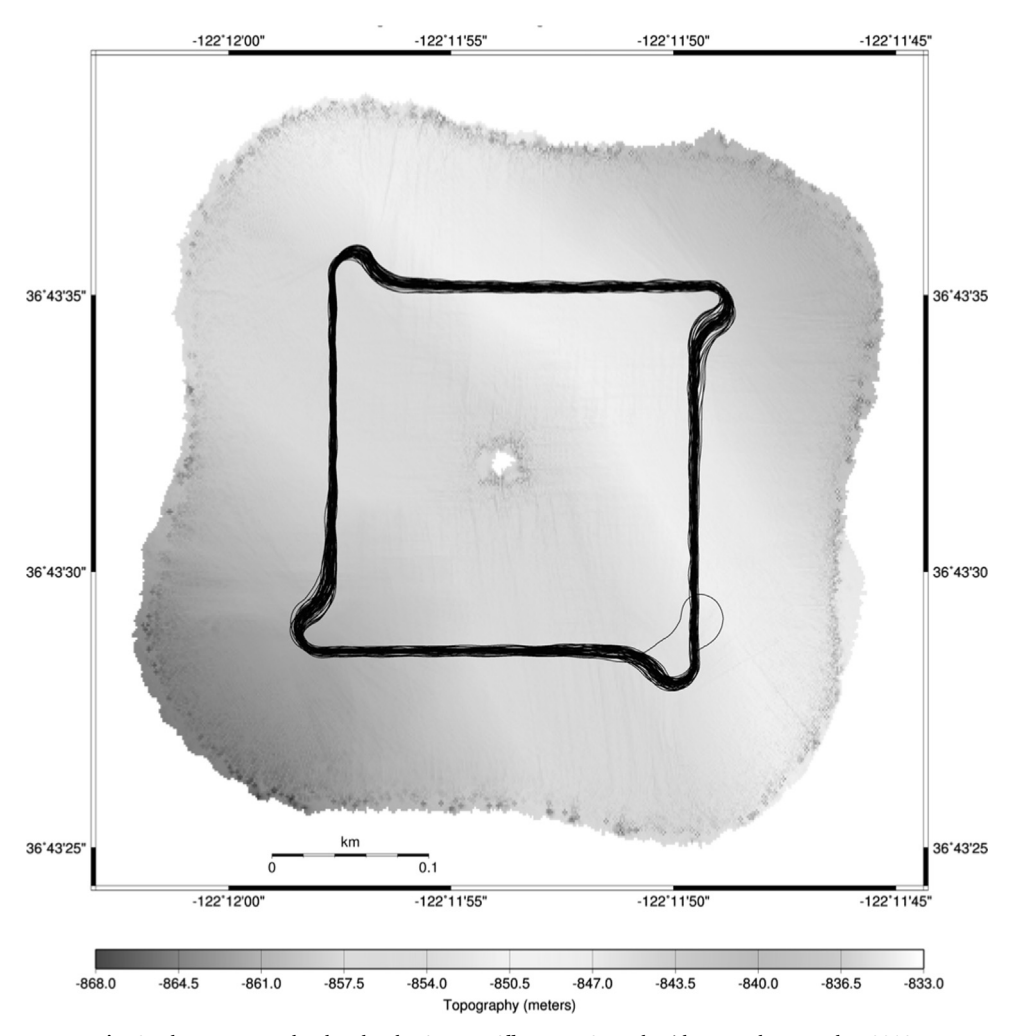


Fig. 2. The survey track taken by the AUV D. Allan B. at Smooth Ridge on 7th November 2012.

where:

calibration methods (i.e. methods for characterising system performance) have been proposed for this instrument (e.g. Lanzoni and Weber, 2011; Wendelboe et al., 2012; Welton, 2014), and it has been shown that it can operate in a linear way under certain conditions (Greenaway and Weber, 2010).

2.3. MBES data processing

A subset of the MBES data (one westward pass of the southern side of the survey track, see Table 1) was processed using Echoview version 7.1 (Echoview Software, Australia), as detailed in Table 2, Fig. 3, the supplementary materials and below. For those interested in the details of processing water-column MBES data, Echoview-specific items are presented in a different font. Extensive details regarding these items can be found in the Echoview Help file, which is publically available both with the software (Help>Contents) and online (Echoview Software, 2016), hence we will describe their application but not their detailed function here.

2.3.1. Data calibration

Data calibration is defined here as the process of establishing, for each sample, the correct location in space and time and the correct backscattering strength. For water-column targets, backscattering strength is typically presented in terms of target strength (TS in dB re 1 m²) for point targets, and volume backscattering strength (S_v in dB re 1 m² m⁻³) for extended (volume) targets (sensu Lurton, 2002).

Despite the caveats around instrument-calibration methods (see

Section 2.2), Echoview 7.1 requires an S_{ν} data type as input for most of its MBES operators. S_{ν} was calculated by Echoview for each sample from the s7k records as follows:

$$S_{\nu} = 20\log_{10}m - t\log_{10}r + 20\log_{10}r + C \tag{1}$$

- m (unitless, linear) is the raw receiver measurement (a data type called multibeam magnitude) for each digitised sample, read from record 7018 and variously referred to as either "magnitude" or "amplitude" (RESON, 2016). This is the "digital number" (dn) described by Welton (2014) that is proportional to receiver voltage (Gorm Wendelboe, pers. comm.) plus a "receiver gain" function calculated by the 6046 acquisition software according to the "TVG formula" $t\log_{10}r + 2\alpha_a r + G_0$ (see below, Table 1 and RESON, 2011 for term definitions).
- *t* (unitless, linear) is a transmission-loss term (spreading-loss coefficient) specified by the user as "spreading" in the 6046 acquisition software and read from record 7000 (Table 1). *t* was left at the 6046 software default of 30 for this survey (the value used in bottom studies for calculating bottom backscattering strength, *S_b* in dB re 1, see Jackson and Richardson, 2007), noting from Eq. (1) that Echoview effectively removes this and replaces it with a value of 20 (the value used in water-column studies for calculating *S_v*);
- r (in m) is the radial range from the transducer to the start of the sample, calculated by Echoview from the sample number based on a start range of 0 m, the sampling rate (in samples s⁻¹) obtained from

Table 1
Key properties of the MBES data analysed in this paper, representing a small subset of *s7k* data files selected from the entire survey dataset. These files included one westward pass (transect) of the southern side of the survey track shown in Fig. 2. Terms, symbols and units are consistent with Demer et al. (2015). ⁿ denotes nominal values (and ^d denotes derivatives thereof) that were not verified for accuracy (i.e. not calibrated). The *s7k* records (see Section 2.2) can be read using the free software utility Echocheck version 8 (Echoview Software, Australia).

Item	Symbol	Value	Units	s7k record (type ^{name})
Number of s7k data files selected	_	5	_	_
Total size of selected files	_	5.02	GB	-
Duration of selected files (total/transect)	_	211/184	S	-
Pings in selected files (total/transect)	_	635/585	pings	-
Transect length (cumulative ping-to-ping distance)	_	143.2	m	-
AUV speed during transect (mean, min-max)	_	0.74 (0.65-0.81)	$m s^{-1}$	-
Ping rate	_	~0.333 (variable)	S	7000 ^{ping period}
Along-track distance between ping centres (mean, min-max)	_	24.5 (19.0-28.5)	cm	_
Number of receive beams per ping	_	256	beams	7004 N; 7018 beams, N
Beamwidth (along-track × across-track)	$\alpha_{-3\mathrm{dB}} \times \beta_{-3\mathrm{dB}}$	$1 \times 0.5^{\rm n}$	deg.	7000 projector -3 dB beam width . 7004^{-3} dB beam width Y/X
Total ping aperture (along-track × across-track)	_	1×128.1^{d}	deg.	-
Range at which subsequent pings overlap	_	44.60 ^d	m	-
Pulse duration	τ	0.000033 ⁿ	S	7000 ^{Tx pulse width}
Sampling rate	_	34,482.76	s ⁻¹	7000 ^{sample rate}
Source level	SL	220 ⁿ (1 m range)	dB re 1 μPa	7000 ^{power selection}
Acoustic transmit centre frequency	f	396,000 ⁿ	Hz	7000 ^{frequency}
Acoustic transmit frequency bandwidth	b_f	0^{n}	Hz	7000 ^{receiver} bandwidth
On-axis gain	G_0	60 ⁿ	dB re 1	7000 ^{gain selection}
Absorption coefficient	α_a	0.039 ⁿ	$dB m^{-1}$	7000 ^{absorption}
Water sound speed	c_w	1481.08 ⁿ	$m s^{-1}$	7000 ^{sound velocity}
Spreading-loss multiplier	ť	30	_	7000 ^{spreading}
Number of samples per beam	_	8149	samples	7018 ^{samples, S}
Number of samples per ping	_	2.086 million	samples	_
Number of samples analysed	_	1.2 billion	samples	-
Ping range	_	175 ⁿ	m	7000 ^{range} selection
Sample thickness in range (along beam axis)	_	2.15 ^d	cm	_
Sample/beam width (along-track × across-track)	_	$1.75 \times 0.97 (1 \text{ m range})^d$	cm	_
		$17.45 \times 8.73 (10 \text{ m range})^d$ $87.27 \times 43.63 (50 \text{ m range})^d$		
Ping width (across-track)	-	4.11 (1 m range) ^d 41.10 (10 m range) ^d 205.48 (50 m range) ^d	m	-
MBES depth (mean, min-max)	-	805.78 (799.76-810.00)	m	_
MBES range above seafloor (altitude) (mean, min-max)	-	55.86 (51.55-61.80)	m	_
Insonified water volume (transect total)	-	874,134.8 ^d	m ³	_

the "sample rate" value in record 7000, the water sound speed (c_w in m s⁻¹) obtained from the "sound velocity" value in record 7000, and the number of samples per beam obtained from the "samples" value in record 7018 (see Table 1);

• C (in dB re 1 m 2 m $^{-3}$) is an offset value (called calibration offset) specified by the user in Echoview to account for the remaining terms in the "sonar" (echosounder) equation for S_{ν} (see Section 4.2.1, Eq. (2)). C was set to 0 for this paper, hence the sample backscattering strengths represented $S_{\nu u}$ (uncalibrated S_{ν}) and ranged in value from (approximately) -10 to +70 dB re 1 m 2 m $^{-3}$.

Each sample was located as accurately as possible in terms of latitude, longitude and depth. The INS latitude/longitude measurements (added as a gps.csv file to a separate fileset) were matched with each MBES ping on the basis of date/time. Each sample was placed in 3D space using the sample ranges (Eq. (1)) and beam-steering angles calculated from the s7k records ("projector beam steering angle vertical/ horizontal" values in radians are available from record 7000), and the transducer geometry values specified under transducer properties (elevation/azimuth/rotation = 0° , XYZ offsets from the GPS = 0 m). Sample locations were adjusted further based on the AUV depth and roll measurements. AUV depth was imported as a line definition file (evl file), and the resulting editable line (which we called "AUV depth") was used as the heave source (specified under platform properties) to define the starting depth for each ping. AUV roll was added as a roll.csv file to a separate fileset, and used as the source data (operand) for the roll-correction operator

(Multibeam Roll at Transducer).

2.3.2. Data cleaning

The Ping Subset operator was used to exclude pings that were collected after the AUV turned north from its westward course. Statistical algorithms were applied to the sample S_{vu} values in the retained pings (by applying operators as detailed in Table 2) to remove reverberation (unwanted backscatter) and noise (both terms sensu Simmonds and MacLennan, 2005) (Fig. 4). The particular algorithms and settings chosen from the range of options in Echoview 7.1 were those that appeared to clean the data most effectively, as verified by visual inspection of the resulting multibeam echograms.

2.3.3. Target detection and tracking

An image-analysis algorithm (the Multibeam Target Detection operator) was applied to the cleaned data to detect contiguous clusters of above-threshold S_{vu} samples in each ping (Fig. 5). Each cluster represented the cross-section of a target at a given point in space and time (where a target is an object with a density sufficiently different to that of the surrounding water, sensu Simmonds and MacLennan, 2005). It was not possible to confirm from the cross-sections whether each target was an individual (such as a single fish or gas bubble) or an aggregation of individuals (such as a school of fish or cluster of bubbles), nor whether it was completely insonified within the MBES swath (a point target, sensu Lurton, 2002) or whether it extended beyond the swath (an extended target, sensu Lurton, 2002) in the along-track dimension (see Section 4.4). The location of each cross-section was defined by Echoview as its geometric centre in the across-track and

Table 2

The MBES data-processing workflow performed in Echoview 7.1 (see also Section 2.3, Fig. 3 and the supplementary materials). Echoview-specific items are presented in a different font. Comprehensive details regarding software function can be found in the Echoview Help file, which is publically available both with the software (Helps Contents) and online (Echoview Software, 2016).

Processing step	Purpose	Description	Key settings
Explore	To establish the broad characteristics of the data in order to inform the optimal processing approach	Visualisation and numerical querying of the data via echorrams, granhs, tables, mans and 4D views	None
Calibrate	To establish the correct location of each digitised sample in terms of latitude lonoitude, ranse from transducer.	AUV INS position fixes used as position source	Platform type: Position determined by GPS Position source. "AUV GPS: nosition GPS fives comma-separated values"
	depth and time (backscattering strength was not calibrated for this study)	AUV pressure-sensor measurements used as heave source Multibeam Roll at Transducer operator applied	Total command of the
		based on the AUV INS roll measurements	
Clean	To remove from the data (1) any measurements made at	Ping Subset operator used to exclude pings from	Ranges: by number: 0-584 (out of 0-634)
	unwanted times or locations, (2) any statistical variation	unwanted times/locations (in this case, off transect)	Include the ping ranges
	in the measurements (statistical noise), (3) any acoustical	Kovesi Image Denoising operator (derived from	Minimum wavelength: 4
	or electrical noise, and (4) any unwanted targets	Kovesi, 1999) used to reduce stochastic variance in the	Softness: 1
	(reverberation) (see rigs. 4 and 0)	sample σ_{yu} values Multibeam Background Remoyal operator used to	standard deviations to reject: 4 Minimum threshold: 25
		estimate and subtract reverberation and noise	Window size (pings): 11
			Algorithm: Median
			Minimum SNR (dB): 15
Detect and track	To delineate (detect) backscattering targets in the water	Multibeam Target Detection operator used to	Specified maximum range (m): 80
	column, to filter these targets as required, and to track	identify and delineate target cross-sections (which could be	Link target clusters: No
	their movement over multiple pings (target tracking) (see	individuals or small aggregations). Note that the target-	Max. horiz./vert. linking dist. (beams/samples): 1.49/1.49
	Figs. 5 and 8)	detection S_{vu} threshold is applied in the previous step	Min. candidate length/height (cm): 0.001/0.001 Min. towart longth/height (cm): 0.001/0.001
		(Multibeam background Removal) Target Commonston chorator used to transform the	Min. carget rengin/neight (cm): 0.001/0.001 Biltor targets: No
		targer conversion operation operation ascar commission are	
		mutibeam-targets echogram (range and across-track distance) into a cinole-beam echogram (range and time)	
		distance) into a single-beam consistent (range and time) prior to filtering and target tracking	
		Processed Data operator used to apply line exclusions	Exclude above line: "DVL-noise max depth"
		(DVL noise and seafloor-generated sidelobe interference	Exclude below line: "Bottom depth directly below MBES (smoothed)"
		between beams)	
		Target Property Threshold operator used to filter	Threshold targets by: Target length across beams (see Table 3)
		target cross-sections based on their properties	Minimum threshold (cm): 0.01
			Maximum threshold (cm): 150
		Target-tracking algorithm (derived from Blackman, 1986)	Single target thickness source/factor: Transmitted pulse length/
		applied to identify detections of the same target over	0.01
		multiple pings (Detect Fish Tracks)	Data: 4D (range, angles and time)
			Alpha (major axis/minor axis/range): 0.4/0.4/0.4
			Beta (major axis/minor axis/range): 0.4/0.4/0.4
			Excl. dist. (m) (major axis/minor axis/range): 1/1/1
			Missed ping expansion (%) (major axis/minor axis/range): 25/25/25
			Weights (major axis/minor axis/range/TS/ping gap): 1/1/1/0.5/0
			Min. no. single targets/pings in track: 2/2
ī			Max. gap between single targets (pings): 3
Characterise	To calculate metrics from the detected and filtered	Analysis By Cells > Fish Tracks (database	Show time/distance grid: GPS distance (m)
	components of the signal (see Figs. 9, 10 and 11)	format) on the Target Property Threshold	Dist. between grid lines (m): 999999
		Target Property Threshold echogram	Separation (m): 9999
		,	Analysis variables to export: All

range dimensions, and the beam axis in the along-track dimension. The S_{vu} threshold for the Multibeam Target Detection algorithm (25 dB re 1 m² m⁻³, see Table 2) was chosen based on visual inspection of the multibeam echograms. Cross-sections were excluded from further analysis (filtered) if their length across beams (LAB; see Table 3) was either 0 cm or > 150 cm and/or they were within the DVL-noise zone (Fig. 4C) or sidelobe-interference zone (Fig. 4F) (defined as range-based exclusion lines). Cross-sections with a LAB of 0 cm were considered questionable as being representative of a biological target (because they were detected in one beam only and hence hard to distinguish from any remaining noise), while visual inspection of the echograms revealed that cross-sections with a LAB > 150 cm were due to the erroneous detection of high- S_{vu} noise artefacts that still remained after cleaning (see Fig. 6 and Section 4.3).

A target-tracking algorithm (called fish tracking and derived from Blackman, 1986) was applied to the filtered cross-sections to identify detections of the same target over multiple pings (tracks). Tracking is intended to characterise the movement of a target in space and time, which assumes that the location of each cross-section in each ping approximates the geometric centre of the target (see Section 4.5). In essence, the algorithm attempts to determine whether or not the space and time difference between point targets in different pings means that those targets are likely to be the same object. Tracks are created based on a sequence of adjustable settings (Table 2) and displayed as 2D polygons (called fish track regions). By specifying at least two cross-sections per track (one of the final stages of the algorithm), cross-sections detected only once were excluded from further analysis. These were considered questionable based on the assumption that a genuine biological point target would likely be seen at least twice at such a rapid ping rate, except if it moved away rapidly in the opposite direction to the AUV.

2.3.4. Target classification

We considered images and videos of benthopelagic animals recorded at the MARS site as additional evidence (sensu Fernandes et al., 2016) to assist with the classification of our detected targets. Many of the species observed in these images and videos have also been recorded from HOVs, baited cameras and midwater trawls in Monterey Canyon (e.g. Anderson, 1980; Eittreim et al., 1989; Yeh and Drazen, 2011), and we assumed that observations here and at the MARS site are representative of our nearby AUV survey site.

2.3.5. Target characterisation

The tracked targets were characterised in terms of their location, size and movement in space and time, and the results (analysis variables) were written to a number of csv files (export analysis). The track characteristics were summarised using spreadsheet software and the volumetric number-density of targets (ρ_{ν} in targets m⁻³) was estimated by echo counting based on a wedge-shaped sampling volume (Kieser and Mulligan, 1984). Erroneous tracks were identified on the basis of anomalous characteristics and re-checked by visualising in three dimensions in Echoview (using the 3D single targets graph), resulting in the removal from the results of one track with an unrealistically high mean speed (15.8 m s⁻¹). ρ_{ν} was calculated as the total number of targets ($\Sigma Targets$) divided by the sampling volume (V in m³). $\Sigma Targets$ was defined as the total number of tracks, and V (Fig. 7) was calculated as the "spherical volume" (sensu Trenkel et al., 2008), being the sum of the ping volumes (ΣV_p) along the transect across all beams between the maximum range of the DVL-noise zone $(R_{dyl-max}, Fig. 4C)$ and the minimum range of the sidelobe-interference zone (R_{s-min} , Fig. 4F).

 $R_{dvl-max}$ was set for every ping to a fixed value of 20 m by applying the Linear Offset line operator to the "AUV depth" line (to create a virtual line that we called "DVL-noise max depth"; see Fig. 3 and Table 2). R_{s-min} was set for each ping to the range of the seafloor directly below the transducer, defined as the range to the maximum S_{vu} value in the nadir (0°) beam. This was calculated by creating a single-beam echogram for the nadir beam using the Angle Select operator, and applying the maximum Sv line pick algorithm (start/stop depth = 850/870 m) to create an editable line that was smoothed with the Smoothing Filter line operator (5-ping median) and called "Bottom depth directly below MBES (smoothed)" (see Fig. 3 and Table 2). V_p for each ping was calculated as the area of the spherical volume in the across-track plane multiplied by the great-circle along-track distance to the next ping (d_p) .

3. Results

3.1. Targets and tracks

A total of 1862 filtered cross-sections were detected, resulting in 366 verified tracks from 1152 cross-sections (Fig. 8). The sampling volume (V) was 411,511.1 m³ (noting from Table 1 that this represents 47% data loss from the water column due to DVL noise and sidelobe interference),

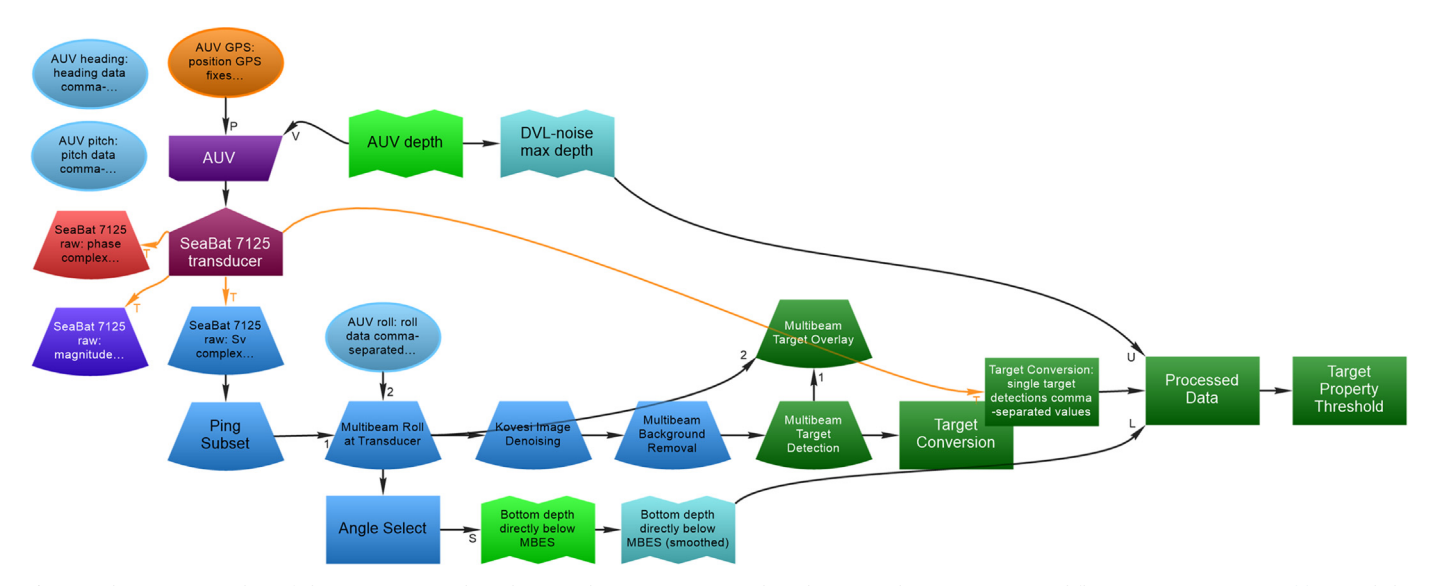


Fig. 3. Echoview screenshot of the dataflow window showing the operators used in the MBES data-processing workflow (see Section 2.3, Table 2 and the supplementary materials).

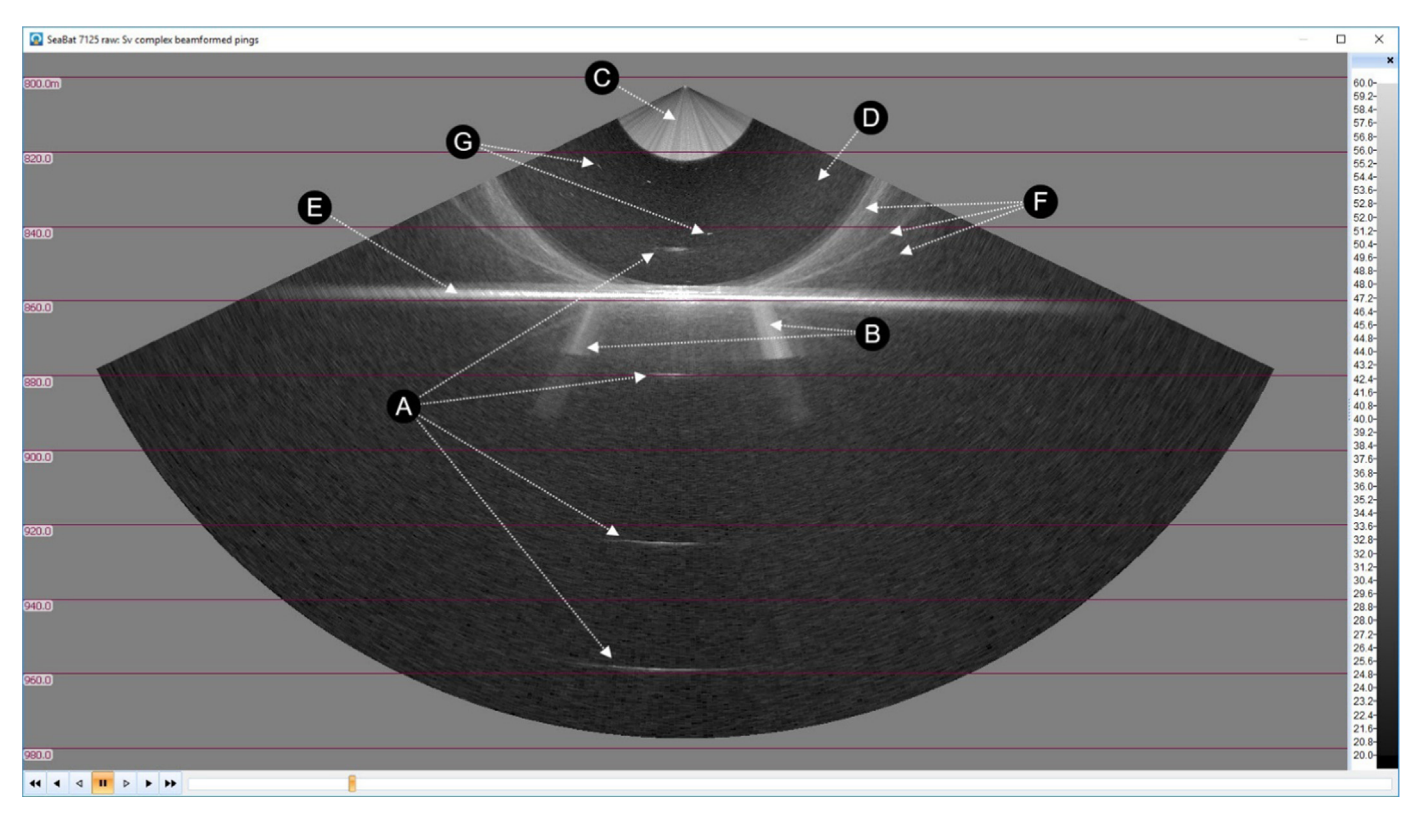


Fig. 4. Echoview screenshot of a multibeam echogram showing the raw beamformed S_{vu} samples from a representative ping (ping 85). Although not visible here, beams are numbered left to right from 0 to 255 (-64.05° to $+64.05^{\circ}$, where 0° is straight down, negative values are to port and positive values are to starboard). [A] Type 1 intermittent noise. [B] and [C] DVL noise. [D] Stochastic variance (statistical noise) in the sample S_{vu} values. [E] Backscatter from the seafloor (reverberation). [F] Seafloor-generated sidelobe interference (reverberation). [G] Biological-target cross-sections (two examples are indicated, but there are others visible). See Sections 2.3.2, 4.3 and 4.4 for further details. The vertical scale represents water depth (D) in m. The ping (swath) width at the seafloor is \sim 235 m. The colour scale represents S_{vu} in dB re 1 m² m⁻³ (see Eq. (1)).

resulting in a volumetric number density (ρ_{ν}) of 0.0009 targets m⁻³ (or 1 target every 1121.3 m³, which is roughly half the volume of an Olympicsize swimming pool). Cross-sections ranged in length (see Table 3 for details regarding this metric and the others described in this section) from 18.3 to 144.8 cm (mean 42.7 cm, CV 54.5%; Fig. 9A). Targets were not tracked for particularly long as the AUV moved over them, with the number of cross-sections per track ranging from 2 to 18 (mean 3.1, CV 61.9%), track lengths from 0.1 to 7.5 m (mean 1.0 m, CV 101.9%; Fig. 9B) and track durations from 0.3 to 7.3 s (mean 0.9 s, CV 98.6%). Very few of the tracks terminated at across-track beam angles near the edge of the swath (i.e. close to -64° or $+64^{\circ}$), indicating that when a target ceased to be detected, it was either beyond the swath in the along-track direction, or within the swath but no longer presenting a detectable crosssection. Tracks were more or less straight, with the tortuosity index (divergence from movement in a straight line) of each track ranging from 1 (a straight line) to 6.9 (mean 1.3, CV 58.6%). Track directions were mostly downwards, away from and ahead of the AUV (which itself was moving in a W direction, i.e. 270° , and descending at $\sim 0.05 \,\mathrm{m \, s^{-1}}$), with 92.9% of the track directions being downward and 79.8% being forward within a 90° quadrant ahead of the AUV (i.e. 225-315°) (Fig. 10). Track depth changes ranged from $-1.0 \,\mathrm{m}$ (i.e. upwards) to $+3.7 \,\mathrm{m}$ (i.e. downwards), and mean track speeds ranged from 0.2 to $4.5 \,\mathrm{m\,s}^{-1}$ (mean 1.1 m s⁻¹, CV 48.2%; Fig. 9C). The mean track speed and horizontal direction was similar to the speed and direction of the AUV due to spatial confounding in the along-track dimension (see Section 4.5). This confounding was less likely to apply to the range dimension, and we interpreted the consistent downward movement of targets as an avoidance response to the AUV (see Section 4.1). The mean S_{vu} of cross-sections within a given track did not vary appreciably from ping to ping (track range in S_{vu} as a percentage of track mean $S_{vu} = 0.04-35.5\%$, mean 8.2%), and there was no obvious relationship between a cross-section's S_{vu} and its across-track angle (Fig. 11A). This indicated relatively little variance in backscatter due to target tilt angle and/or location within the MBES swath. Tracked-target depths ranged from 814.7 to 859.1 m (mean 833.7 m, CV 1.1%), and from 2.6 to 43.4 m above the nadir-beam seafloor depth (mean 26.4 m, CV 31.9%) (Figs. 9D and 11B).

3.2. Target classification

Of the species observed by cameras at the MARS site, those within the approximate size range of our detected cross-sections include the giant grenadier (*Albatrossia pectoralis*), Californian slickhead (*Alepocephalus tenebrosus*), sablefish (*Anoplopoma fimbria*), finescale antimora (*Antimora microlepis*), twoline eelpout (*Bothrocara brunneum*), Pacific grenadier (*Coryphaenoides acrolepis*), Humboldt squid (*Dosidicus gigas*), eelpout (*Lycodapus* sp.), North Pacific hake (*Merluccius productus*) and filetail catfish (*Parmaturus xaniurus*). Of these species, Californian slickhead, finescale antimora, Pacific grenadier, Humboldt squid, eelpout and North Pacific hake (Fig. 12) have been commonly observed within the range of altitudes recorded for our detected targets (from 2.6 to 43.4 m off the seafloor; Fig. 9D) and were therefore potential candidates, with the remaining species typically being observed within 2 m of the seafloor. Details of species observations at the MARS site are provided in the MBARI Deep-Sea Guide (Jacobsen Stout et al., 2016).

4. Discussion

As a proof of concept, the results provide an indication of the information that can be extracted from MBES water-column data collected in the deep-sea BBL. Our methods, which can be adapted as required to water-column MBES measurements from different environments and MBES systems, followed a logical workflow for echosounder data processing and were subject to familiar computational challenges (e.g. Buelens et al., 2006; Gee et al., 2012). In any

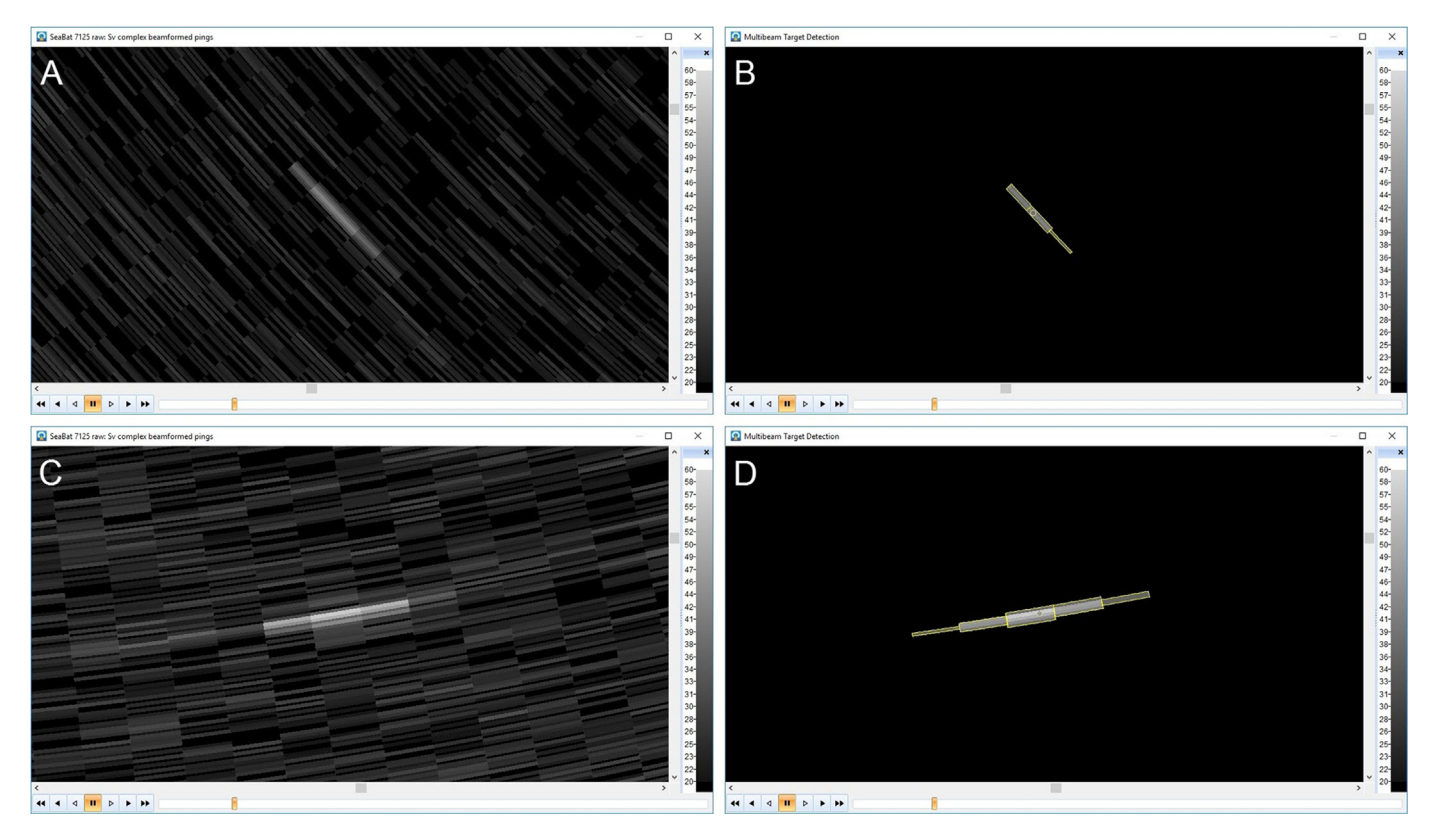


Fig. 5. Echoview screenshots showing zoomed views of the two biological-target cross-sections indicated by arrows in Fig. 4G (and see Section 2.3.3). The panels on the left represent the raw data and those on the right represent the results of the Multibeam Target Detection operator. [A and B] An average-sized cross-section spanning 3 beams at 31.7 m range: depth = 824.5 m; across-track angle = -44.8° ; total length (to the beam edges) = 83.9 cm; length across beams = 55.3 cm; mean $S_{vu} = 38.7$ dB re 1 m² m⁻³. [C and D] A large cross-section spanning 5 beams at 40.4 m range: depth = 841.6 m; across-track angle = $+11.2^\circ$; total length (to the beam edges) = 181.0 cm; length across beams = 141.6 cm; mean $S_{vu} = 47.5$ dB re 1 m² m⁻³. The colour scale represents S_{vu} in dB re 1 m² m⁻³ (see Eq. (1)).

Table 3

The metrics used to characterise tracked targets (Echoview-specific items are presented in a different font). These metrics are referred to as analysis variables in Echoview, and were calculated by performing two different types of export analysis on the Target Property Threshold echogram shown in Fig. 3.

Metric (as described in Section 3.1)	Echoview analysis variable used
Cross-section length	Target length across beams ^a
Number of cross-sections per track	Num_targets ^b
Track length	Distance_3D_unsmoothed ^b
Track duration	Time in beam ^b
Track tortuosity index	Tortuosity_3D ^b
Track movement downward	Direction_vertical ^b
Track movement forward	Direction_horizontal ^b
Track depth change	Fish_track_change_in_depth ^b
Mean track speed	Speed_4D_mean_unsmoothedb
Track range in S_{vu}	TS_min ^b
	TS_max ^b
Track mean cross-section S_{vu}	TS_mean ^b
Cross-section across-track angle	Angle_major_axis ^a
Target depth	Target_true_depth ^a

a Denotes export-analysis type Analysis By Cells>Fish Tracks, with the export type set to Database format (multiple files); the file subsequently used was the "...(targets).csv" file.

echosounder-based study, it is important to consider how the acoustic metrics relate to the structure and function of the ecosystem that we wish to understand (see e.g. Bertrand et al., 2003; Trenkel and Berger, 2013; Benoit-Bird and Lawson, 2016), which requires a

detailed understanding of the data from collection through to characterisation.

4.1. AUV-based data collection

The tools used to date to study deep-sea benthopelagic animals are known to have a range of limitations (Raymond, 2008). Trawls can be destructive to the environment and to the captured specimens, are prone to avoidance or herding artefacts, and provide limited information on animal behaviour; HOVs and ROVs typically generate light and noise that can cause physiological damage to animals and influence their behaviour; camera sleds generate light and yield no physical samples; baited landers are limited to providing information on scavenger species; and they all sample only a relatively small volume of the environment (e.g. Cailliet et al., 1999; Jones et al., 2003; Widder et al., 2005; Mann et al., 2008). The use of AUVs as survey platforms promises to address some of these limitations. However, there remains the potential for observer bias in the form of animal avoidance or attraction, which is clearly undesirable when wishing to accurately describe the natural distribution and swimming behaviour of animals. In our data, the consistent movement of targets downwards away from the AUV (Fig. 10) was indicative of avoidance (and see Section 4.5). For an MBES, orientation changes in targets relative to the MBES (as they move in a polarised orientation towards or away from the MBES and/or across beams with different steering angles) can cause significant changes in their backscattering strength (particularly those in the Rayleigh scattering regime, where the target size is closer to the acoustic wavelength), and this can influence the ability to detect them above the background noise level (Cutter and Demer, 2007). However, as noted in Section 3.1, there was no evidence of such changes in this dataset.

b Denotes export-analysis type Analysis by Regions > Fish Tracks. Details regarding the calculation of each analysis variable can be found in the Echoview Help file, available both with the software (Help > Contents) and online (Echoview Software, 2016).

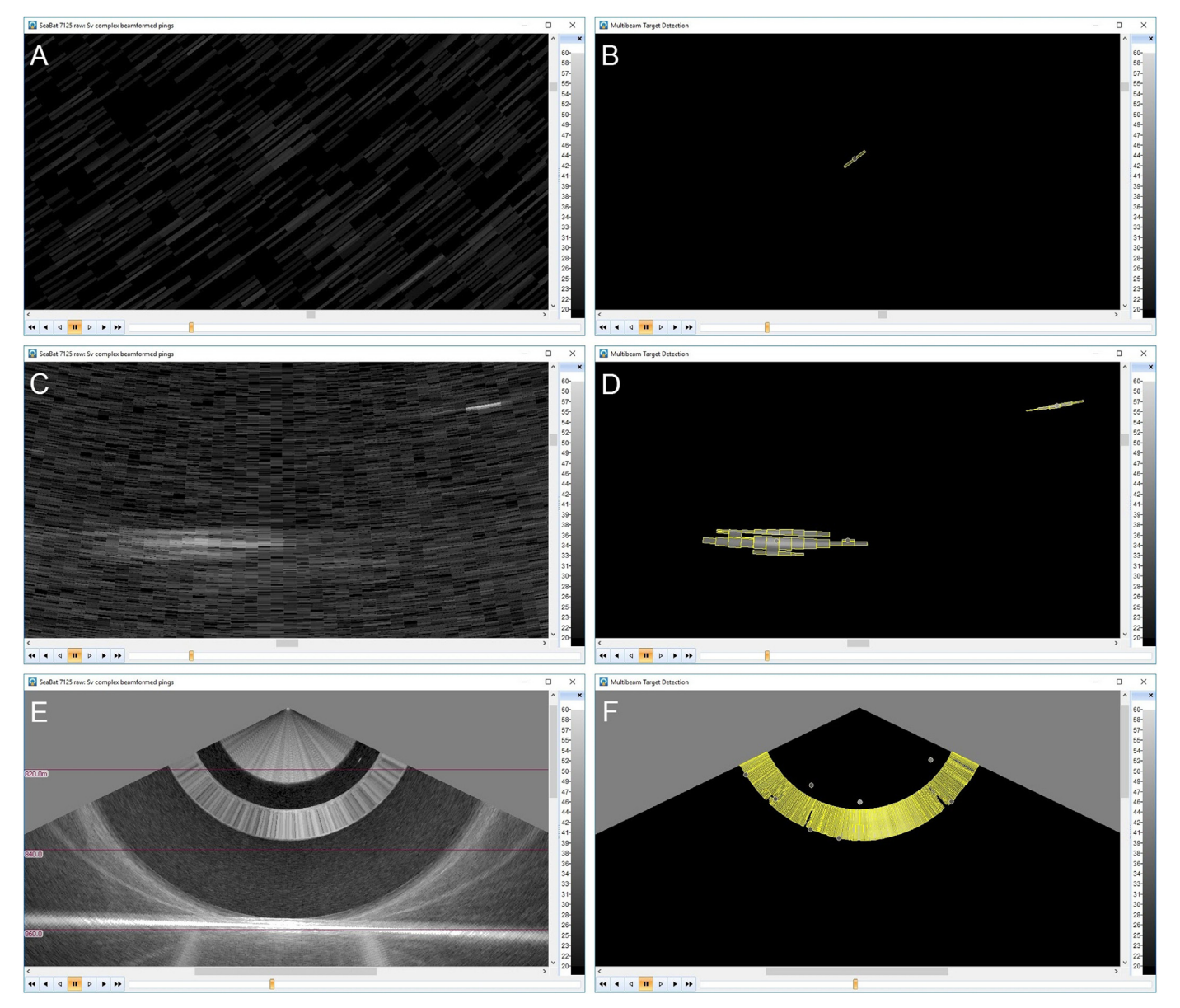


Fig. 6. Echoview screenshots showing examples of three false (i.e. non-biological) target cross-sections (see Section 2.3.3). The panels on the left represent the raw data and the panels on the right represent the results of the Multibeam Target Detection operator. [A and B] A false cross-section in ping 85 that spans a single beam and was subsequently filtered out on the basis of size (length across beams = 0 m). [C and D] A false cross-section in ping 85 (visible as the large cross-section in the lower half of each panel) that represents the type 1 intermittent noise described in Section 4.3 and indicated in Fig. 4A. The smaller cross-section in the upper right is the one shown in Fig. 5C-D. [E and F] A false cross-section in ping 200 (visible as the large annulus spanning across all beams) that represents the type 2 intermittent noise described in Section 4.3. The colour scale represents S_{vu} in dB re 1 m² m⁻³ (see Eq. (1)).

The most likely cause of avoidance behaviour in response to a survey platform is radiated noise, but the perceived gradient of the acoustic pressure, visual cues, bow waves, particle acceleration and stimulated bioluminescence have also been suggested (De Robertis and Handegard, 2012). A number of studies have considered the response of animals to AUVs (e.g. Patel et al., 2004; Tolimieri et al., 2008; Guihen et al., 2014), but our results represent the first record, as far as we are aware, of potential AUV avoidance by animals in the deep sea. Avoidance behaviour in the deep sea has been observed in sablefish (Anoplopoma fimbria) "and other species" in Monterey Bay in response to an ROV, thought to be caused by the radiated noise from the hydraulic propulsion (Stoner et al., 2008). The D. Allan B. was not configured with lights, and the source level from the propulsion and steering (measured in 2009 while passing within approximately 25 m of a Greeneridge Sciences Bioacoustic Probe hydrophone) was below 90 dB re 1μPa at 1 m range (cf. 124 dB for the "exceedingly quiet" AUV Autosub and ~155 dB for the noise-reduced

research vessel *Scotia*; Griffiths et al., 2001). Additional experiments will be required to determine which aspects of the *D. Allan. B.* are responsible for any observed responses by animals. If noticeably different responses are apparent between species, the characteristics of the response could be used to assist in classifying targets (e.g. Spampinato et al., 2010).

4.2. Data calibration

For water-column MBES studies, calibrated samples (see Section 2.3.1) can enable greater accuracy when quantifying the abundance, distribution, size and behaviour of targets such as fish and gas bubbles. If for practical reasons it is not possible to achieve calibrated data (a common situation for MBES surveys), there will be greater uncertainty in the results, but the majority of MBES water-column studies to date (including this one) have demonstrated that uncalibrated data can still provide valuable ecological information (e.g. Colbo et al., 2014; Kupilik and

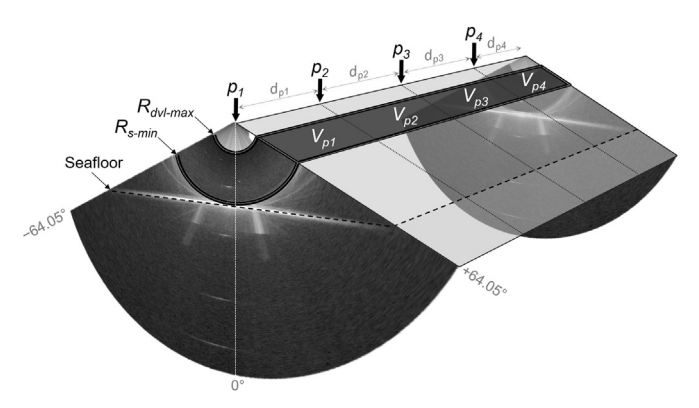


Fig. 7. The sampling volume, V, for four consecutive pings (p_1 to p_4), based on the "spherical volume" described by Trenkel et al. (2008) and the "wedge-shaped volume" described by Kieser and Mulligan (1984). See Section 2.3.5 for details. Note the exaggerated along-track scale for illustrative purposes.

Petersen, 2014). Nevertheless, there is significant interest in calibration methods for existing MBES systems (e.g. Demer et al., 2015), as well as the development of new systems that can be more easily characterised. Hence we turn now to a discussion of data calibration for the SeaBat 7125.

4.2.1. Abundance

When a target represents aggregated individuals (see Section 4.4), echo integration is the technique used to estimate the abundance of those individuals (Foote, 1983; MacLennan et al., 2002). This technique

requires accurate (i.e. calibrated) measurements of S_{ν} for each sampling volume, along with an accurate estimate of TS for a representative individual in those volumes. In contrast to SBES and MBES systems with split-beam transducers, phaseless and potentially non-linear MBES systems such as the SeaBat 7125 (that are not designed for quantitative application and are unable to measure the off-axis location of a calibration reference target within each beam) are more challenging to calibrate (e.g. Melvin et al., 2003; Foote et al., 2005; Lanzoni and Weber, 2011), while the assessment of representative TS is a complex task (e.g. Ona, 1999) that is compounded further for MBES data due to the greater range of angles (and sometimes frequencies, e.g. Trenkel et al., 2008) at which the targets are insonified (Cutter and Demer, 2007; Cutter et al., 2009).

When the abundance of aggregated individuals (and hence S_{ν}) is sought, quantification of S_{ν} from the echosounder's raw transceiver measurements requires access during data processing to all of the parameters required to solve the echosounder equation for volume backscattering. When the raw transceiver measurements are considered in terms of received electric power (P_{er} in dB re 1 W), this equation takes the form (after Demer et al., 2015):

$$S_{v} = P_{er} + 20\log_{10}r + 2\alpha_{a}r - 10\log_{10}\left(\frac{p_{et}\lambda^{2}g_{0}^{2}c_{w}\tau\psi}{32\pi^{2}}\right) - 20\log_{10}\left(\frac{\tau_{eff}}{\tau}\right)^{0.5}$$
(2)

If we compare Eqs. (1) and (2), it becomes clear for SeaBat 7125 data that we need to understand the relationship between m and P_{er} (or other suitable proxy for the acoustic pressure in front of the transducer) if we are to calculate S_v from m using accurate (i.e. calibrated) parameters. We know (Gorm Wendelboe, pers. comm.) that a frequency-

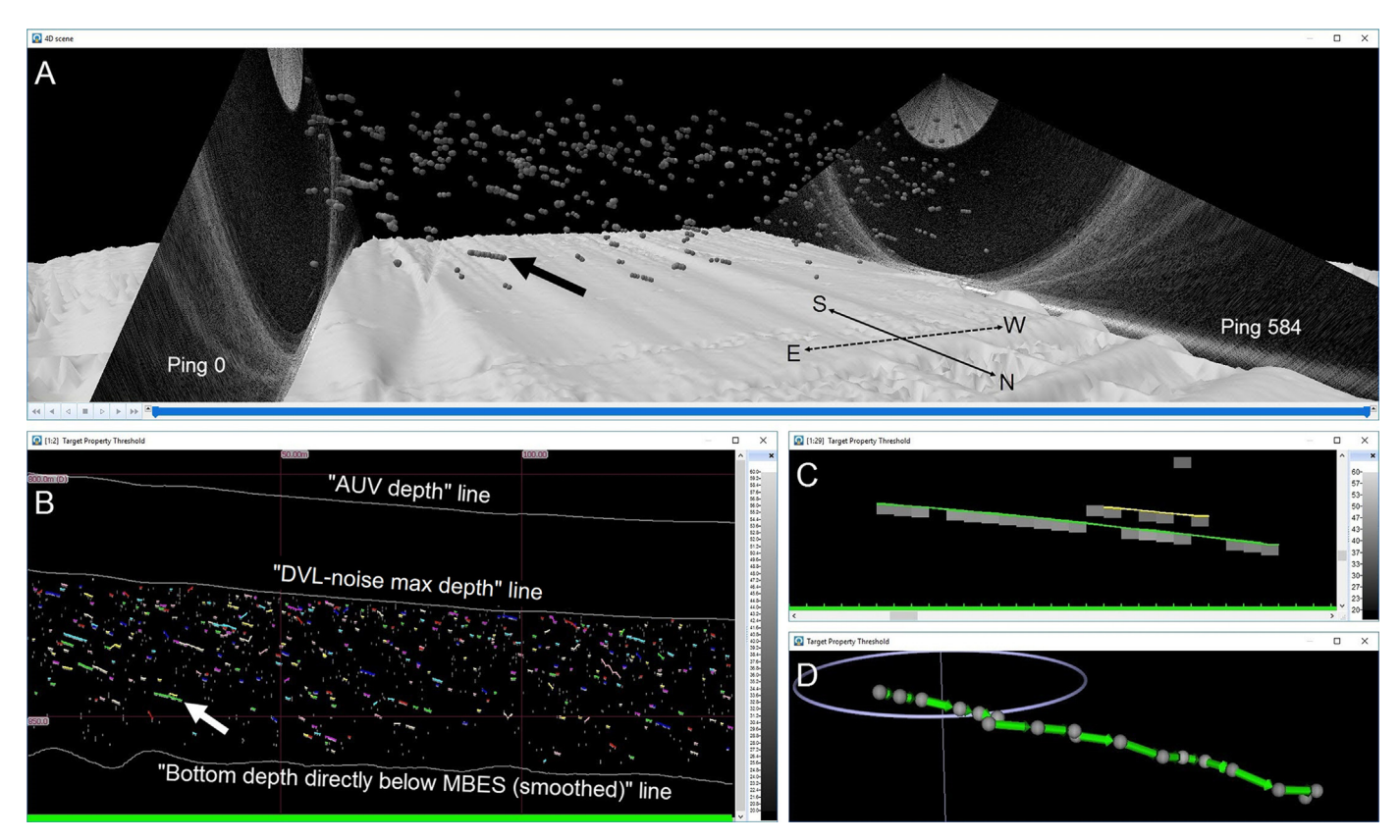


Fig. 8. Echoview screenshots showing the biological-target cross-sections detected in each ping and their tracks (see Section 2.3.3). The bold arrow in panels A and B indicates the same track (at \sim 11° across-track) that provides the focus for panels C and D. [A] 3D view (scene). Pings 0 and 584 are shown for context. The seafloor surface was generated from the data using the multibeam bottom detection algorithm. [B] 2D view (single targets echogram) with along-track distance on the x-axis and depth on the y-axis. Cross-section depths are displayed as their range transposed onto the nadir beam. [C] Zoomed 2D view (single targets echogram) of the track indicated in panels A and B (lower track). The upper track is at a similar range but different across-track angle (\sim 50°). The cross-sections are shown with a range extent of half a pulse length. [D] Zoomed 3D view (3D single targets graph) of the track indicated in panels A and B. The nadir beam axis and beam width (not to scale) are shown for context. The colour scale represents S_{vu} in dB re 1 m² m⁻³ (see Eq. (1)).

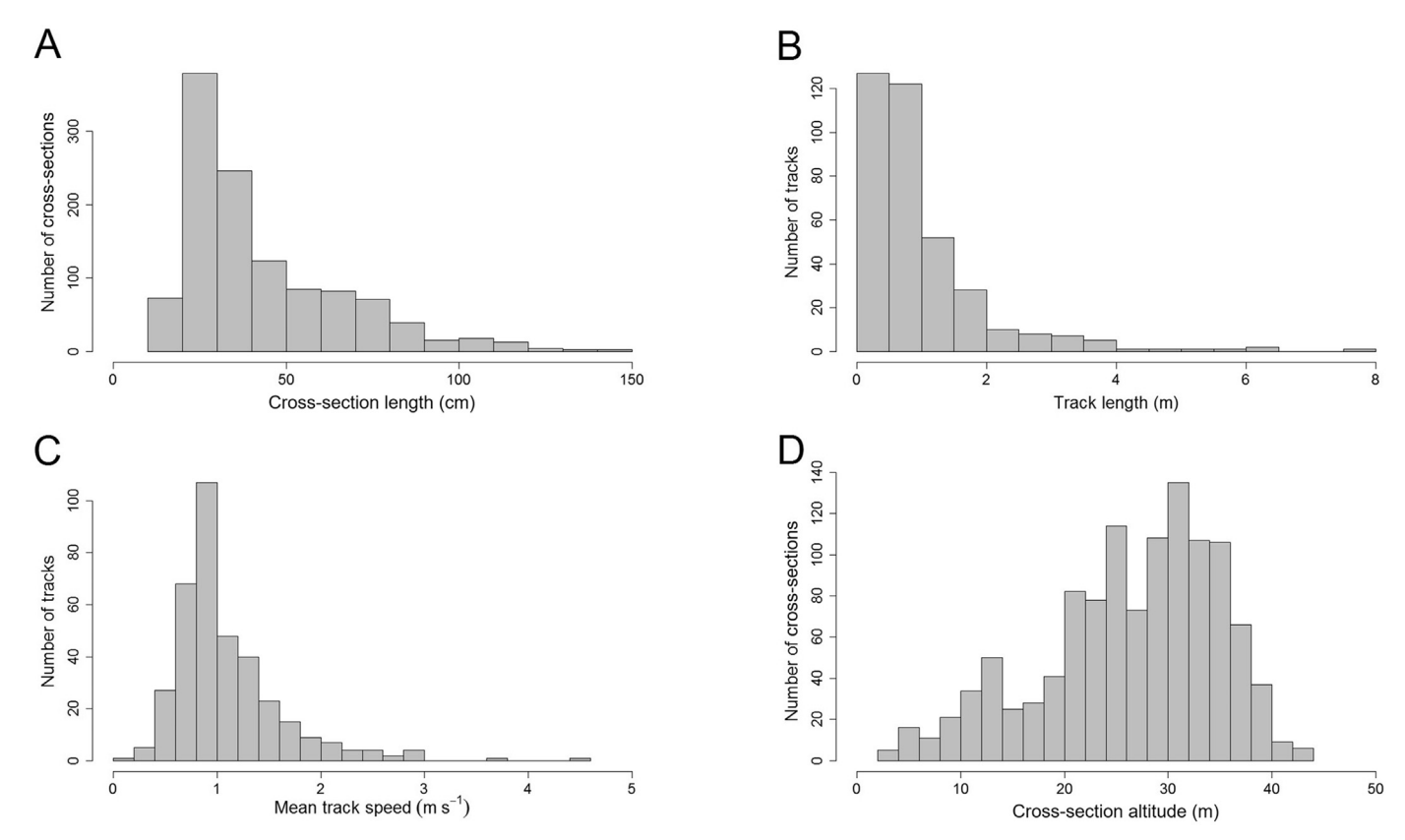


Fig. 9. Histograms of selected tracked-cross-section and track metrics. Altitude refers to the vertical distance of the cross-section above the seafloor. See Table 3 for details regarding each metric. The track metrics are likely affected by spatial confounding (see Section 4.4).

dependent scaling factor is required to relate m to the acoustic pressure in front of the hydrophone, but we do not have further details on how to calculate the value of this factor for a given frequency, or how the digitised voltage is derived from the analog voltage (whether as the peak amplitude, the normalised integral or something else). We also know (RESON, 2016) that the m value from the 7018 record is an unsigned 16-bit integer, meaning that it can range from 0 to 65,535 (i.e. $2^{16} - 1$). Given that power is proportional to voltage squared, we can speculate on how to calculate P_{er} from m:

$$P_{er} = 20\log_{10}\left(m_{rec}C_f\left[\frac{p_{er,max} - p_{er,min}}{2^{16} - 1}\right] + p_{er,min}\right) - t_{rec}\log_{10}r_{rec} - 2\alpha_{a,rec}r_{rec} - G_{0,rec}$$
(3)

where C_f is the frequency-dependent scaling factor, $p_{er,max}$ and $p_{er,min}$ (in W) represent the dynamic range of the receiver, and the subscript rec denotes values obtained from the s7k records. This value of P_{er} could then be used in Eq. (2) to replace Eq. (1).

4.2.2. Distribution, size and behaviour

MBES systems with very narrow beams (which include "imaging sonars" and high-resolution "swath" systems) offer the possibility of reliably detecting small (cm scale) individuals and aggregations across multiple beams at the same time. Their cross-sectional dimensions can therefore be measured directly if the beamwidths are known (e.g. Malzone et al., 2008), hence it is important to accurately know the location (latitude, longitude, range and depth) and volume/extent (range extent, beam width) of each MBES sample to quantify target distribution, size and behaviour. It is important to note that the robustness of size measurements of individual animals, and the relationship of these measurements to total length, is a function of beamwidth, range, orientation and signal-to-noise ratio (Hightower et al., 2013).

Regarding sample latitude and longitude, the INS positional drift

is < 0.05% of the distance travelled when the DVL can detect the bottom. It was straightforward during data processing to match the INS position measurements to each MBES ping based on time, and to offset each sample based on range and beam-steering angle. Regarding sample range, Eq. (1) shows that it is not currently possible for the user to adjust r as a function of c_w during data processing (should a different value of c_w be required to the one entered in the acquisition software), but this adjustment could be easily achieved from the s7k records available. Regarding sample depth (D), in this study we were able to account for ping-to-ping changes in transducer depth and roll, but not pitch and yaw. The requirement to comprehensively account for transducer motion (attitude) will vary depending on the accuracy requirements of the survey and the capabilities of the echosounder (some MBES systems are capable of performing real-time motion correction, see e.g. Trenkel et al., 2008), consideration of which should be made at the survey-design stage to determine what sensors are required (depth, roll, pitch, heading) and whether or not their measurements need to be incorporated when processing the data. While a high level of positional accuracy may not be critical for many surveys, the requirement to accurately account for ping-to-ping changes in attitude, and even decoupled transducer and platform movements, looks set to increase as new sensor-platform combinations become available and survey designs become more dynamic and complex (Dickey et al., 2008; Moline and Benoit-Bird, 2016). Regarding sample volume/extent, in this study we applied only nominal values for the parameters required to calculate sample range-extent and beam width (c_w , τ , $\alpha_{-3\,\mathrm{dB}}$ and $\beta_{-3\,\mathrm{dB}}$; Table 1). While these values were likely to have been relatively accurate, variation from their true value will have introduced error into any size measurements made (and see Section 4.4).

4.3. Data cleaning

Reverberation and noise are common in echosounder data (e.g.

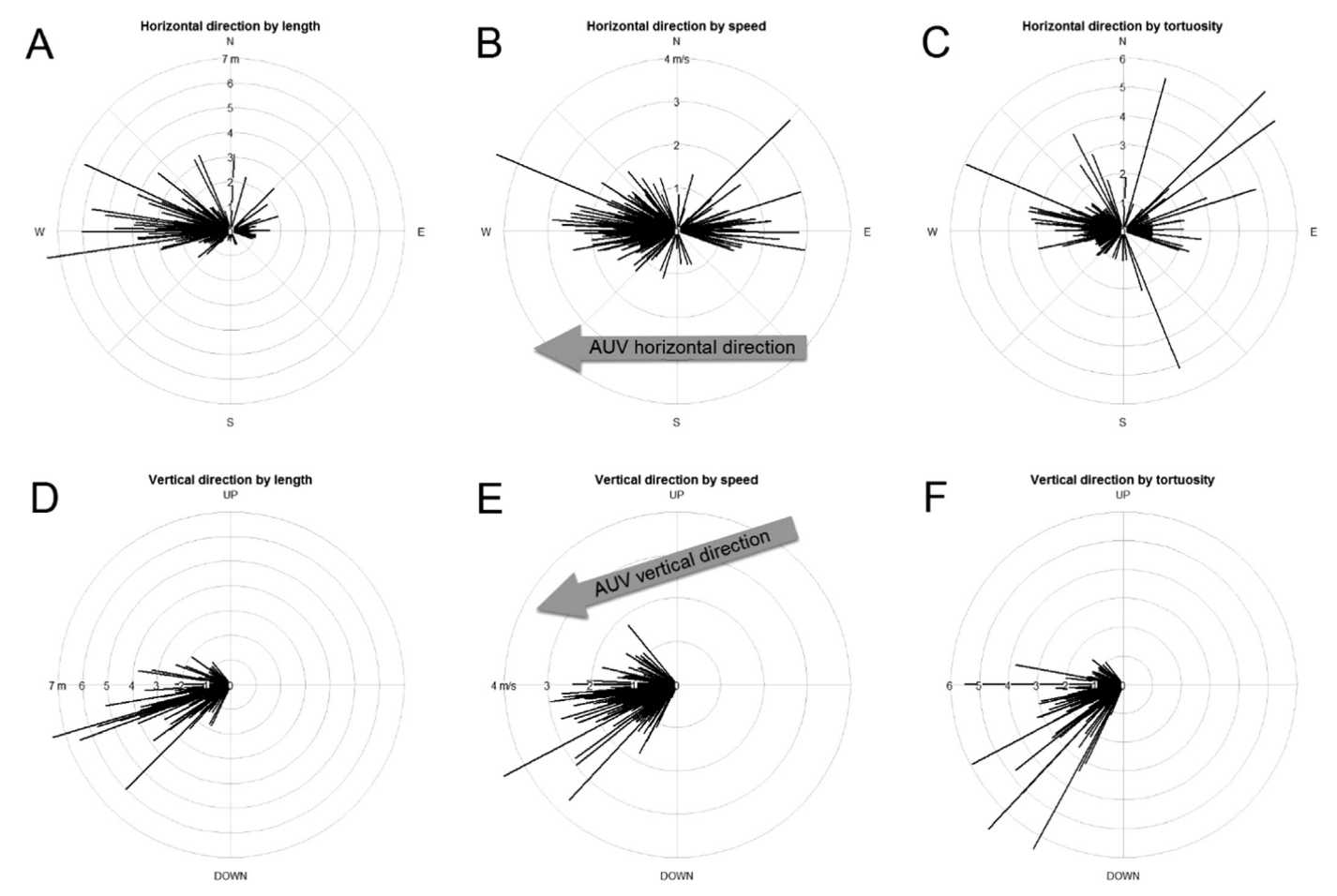


Fig. 10. Polar plots of selected track metrics. See Table 3 for details regarding each metric. The horizontal directions are likely affected by spatial confounding (see Section 4.4), while the consistent downward vertical directions are indicative of an avoidance response by targets to the AUV (see Section 4.1).

Peña, 2016), and examples of each were noticeable in this dataset (Fig. 4). Two types of high- S_{vu} intermittent noise were apparent (Figs. 4A and 6C-F). Type 1 noise (Figs. 4A and 6C-D) was visible across beams ~114–127 (i.e. -6.78° to -0.25° across-track angle), with a duration of ~0.5 ms and a rate of ~20 ms (~50 Hz). There were no sources of 50 Hz alternating current (AC) in operation on the AUV, hence we cannot explain this as electrical interference. While the propeller did rotate with a frequency of roughly 50 Hz, it is unclear how this might have generated short pulses of ~400 kHz sound in the direction of beams 114–127 only. Type 2 noise (Fig. 6E-F) was visible across all beams, with a duration of ~5 ms and a rate of ~15 s (~0.1 Hz). This was likely due to the USBL beacon, which was interrogated by the surface vessel every ~15 s for the first 25 min of the

survey. The MBES hydrophone is located within the near field of the beacon, which transmits a square wave over a wide frequency band that includes the receive band of the MBES. A time-based subtraction algorithm (the Multibeam Background Removal operator; see Table 2) worked to remove some of the samples affected by type 1 and 2 noise, but the intermittent nature of these noise signatures rendered them temporally similar to the detected biological-target cross-sections, and a large proportion of the affected samples remained as contiguous clusters of high- S_{vu} samples (Fig. 6D and F). Being larger than the biological-target cross-sections, these clusters were easily filtered out after detection on the basis of size (see Section 2.3.3).

The noise signatures visible in Fig. 4B and C occurred in every ping and were likely to have been due to the DVL. The DVL was synchronised

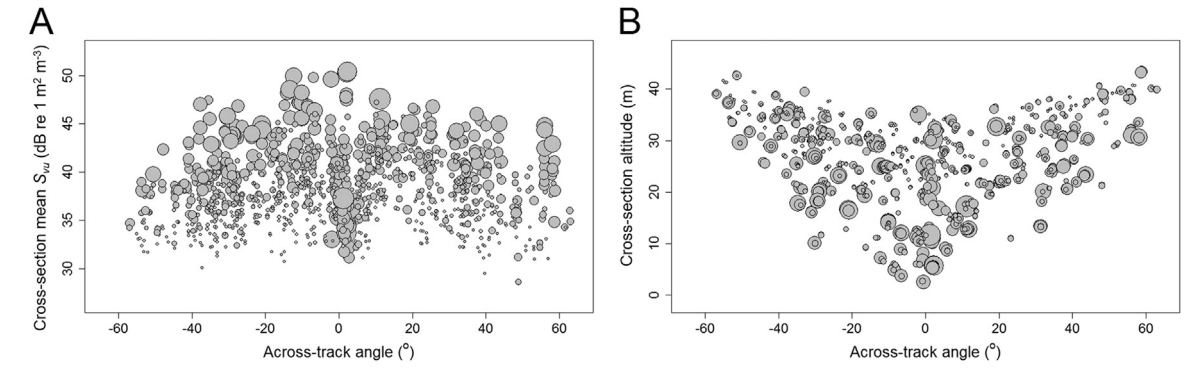


Fig. 11. Scatterplots of selected tracked-cross-section metrics. Altitude refers to the vertical distance of the cross-section above the seafloor. The symbol size represents cross-section length across beams (smallest to largest = 18.3–144.8 cm). See Table 3 for details regarding each metric.

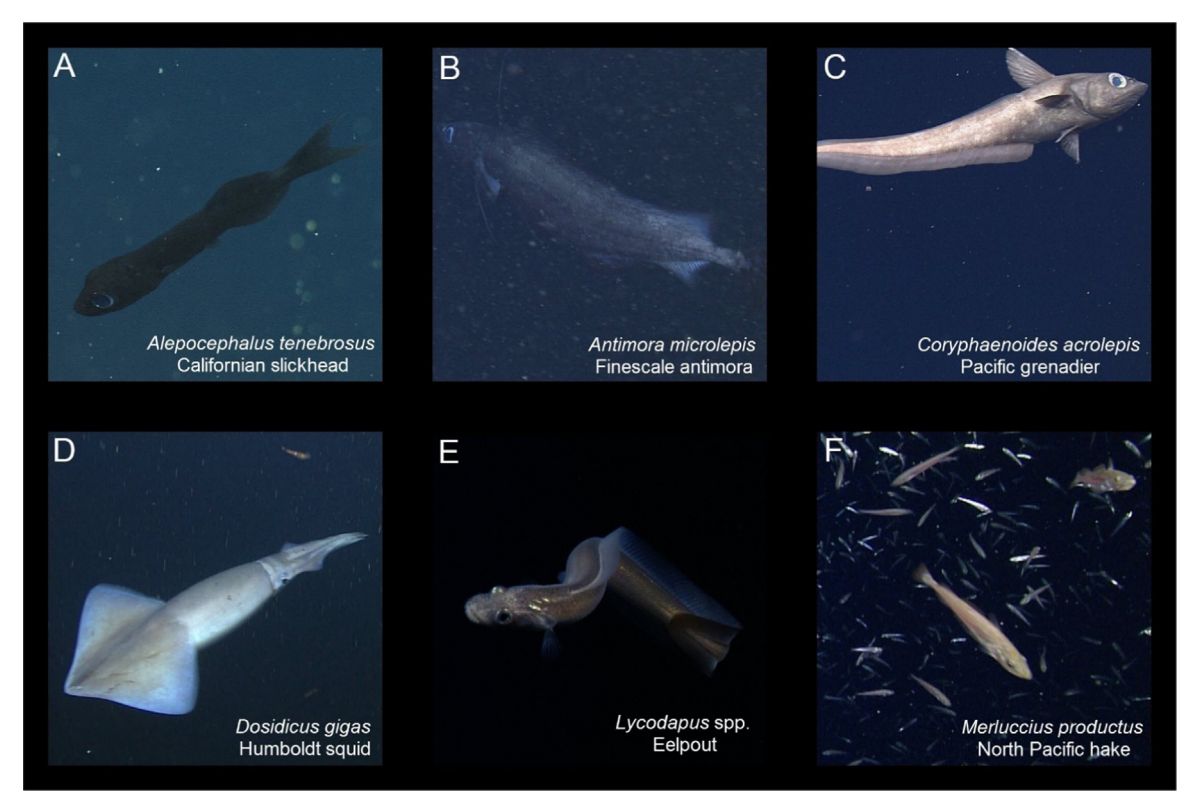


Fig. 12. Video frame grabs from the MARS site of fish and squid species that have been observed within the size range and altitude range of cross-sections detected by the MBES during this study.

to ping at the same time as the MBES, but the square transmit pulse of the DVL is long (relative to the MBES pulse) and variable, and generates considerable sound energy over a wide frequency band that includes the receive band of the MBES. Although the close-range DVL-noise component (Fig. 4C) was easily accounted for using a combination of the Multibeam Background Removal operator and a fixed-range exclusion line, it did result in the loss of information within 20 m of the hydrophone. This noise can be avoided by switching off the DVL during MBES survey operations, but this comes at the cost of reduced positional accuracy.

The natural stochastic fluctuations in backscatter measurements are a common concern for accurate multifrequency sample comparison in SBES data (e.g. Korneliussen et al., 2008), but the focus with this dataset was to improve the detectability of targets of interest (which were marginal in size relative to the MBES sampling resolution; see Fig. 5 and Section 4.4) by enhancing their contrast from the background. Resampling and smoothing are two common techniques to remove statistical noise (see e.g. Peña, 2016 and references therein), and may well have worked effectively with this dataset, but we chose to apply a wavelet-based technique (using the Kovesi Image Denoising operator, after Kovesi, 1999) due to its ability to reduce stochastic variance while leaving the S_{vu} value of target samples untouched.

Most of the MBES systems currently used for water-column studies suffer from sidelobe interference (see Andersen et al., 2006 for a notable exception), which can completely mask targets of interest (see Figs. 4, and 1a in Trenkel et al., 2008). This reduces the available sampling volume close to strongly-reflective targets such as the seafloor, and should be taken into account when interpreting MBES-based measurements of target distribution (e.g. Figs. 9D and 11B). Weber et al. (2009) describe a range-based threshold algorithm for the removal of sidelobe-affected samples, while we used the Multibeam Background Removal operator, which is a time-based subtraction algorithm (Table 2). This operator also served to remove some of the intermittent noise (Fig. 4A), most of the DVL noise (Fig. 4B and C) and

the backscattering from the seafloor (Fig. 4E). Algorithms for the mitigation of sidelobe-affected samples (Fig. 4F) may vary in their efficacy depending on the data, and mostly serve to reduce the potential for spurious target detections rather than reveal targets within the affected samples (since the target backscattering strengths are often significantly weaker than the noise level). Ultimately, solutions for reverberation and noise should be sought via improvements to the survey setup and design and/or the hardware, rather than through data processing.

4.4. Target detection

In order to discern whether a detected cross-section represents an individual (such as a single fish) or an aggregation of individuals (such as a school of fish), it is necessary to consider the size, dispersion and movement of the individuals in the context of the sampling resolution of the echosounder, their orientation relative to the transducer (which is notoriously difficult to know) and any additional evidence (trawl, video etc.). The nominal sample resolution of our MBES data (the volume represented by a single sample) was 2.15 cm along the beam axis and range-dependent across the beam axis (e.g. 1.75×0.97 cm at 1 m range, 87.27×43.63 cm at 50 m range; Table 1). With MBES data, the sample resolution is not necessarily equivalent to the ability to reliably identify target cross-sections; even though it is possible to detect a target that is smaller than an individual beam, a cross-section ideally needs to span multiple beams (maybe 3 or more) if we are to confidently discriminate it from noise. Moreover, the range-dependent nature of the horizontal sample resolution (due to beam spreading) introduces a range-dependent bias to the accuracy of a cross-section's across-track measurement (due to "spatial smearing"; Vatnehol, 2016). For example, the cross-sections of fish ranging from 22 to 66 cm long and oriented in the across-track dimension would all extend completely across 3 beams at a range of 25 m, and hence appear the same on the echogram. At a range of 50 m, the fish lengths would range from 44 to 132 cm to extend across 3 beams, and so on. Processing of this dataset

demonstrates that the reliability of target identification declines with increasing range from the transducer. This can be mitigated by mounting the echosounder on an AUV and bringing the transducer closer to the target (see e.g. Benoit-Bird et al., 2017 for an SBES example).

4.5. Target tracking vs. scanning

In order to track an individual or an aggregation, it is necessary to follow its geometric centre over space and time. This is possible for point targets (sensu Lurton, 2002), especially when locational accuracy is improved using split-beam techniques (typically for SBES data) and/or narrower beams (typically for MBES data, until the beams start to become narrower than the target in the along-track dimension). When tracking in situations where there are extended targets (sensu Lurton, 2002), spatial confounding becomes an issue as the target size increases relative to the beam width. This is because it becomes harder to equate the location of the detected cross-section with the geometric centre of the target at any given point in time.

In our data we were unable to robustly determine whether a detected cross-section was from a point target or an extended target, because the cross-sections were small relative to the sample resolution. Hence we were unable to recognise shapes that might help us discern individuals from aggregations in order to gauge the likely along-track scale, so it was not possible to unambiguously determine whether we were tracking the movement of the target through space and time, or whether we were scanning through its spatial extent. Given the deepsea environment and the MBES beam widths, most of the cross-sections were likely to have been from individual fish or squid in the 20-150 cm length range. These would therefore have been either point targets (i.e. completely insonified within the beams of the swath) or slightly extended targets (meaning that tracking was an appropriate approach), but it is still possible that a proportion of our 'tracks' actually approximated the spatial extent of extended targets. Perhaps of greater concern, the inability to position cross-sections in the along-track dimension anywhere other than the beam axis meant that there was a significant autocorrelation bias between the along-track direction of each track and the movement of the AUV. This was further complicated by any heading changes in the AUV, which cause the MBES swath to swing and the individual beams to move in different vectors.

When wishing to track a point target or scan through an extended target, the first step is to detect the target cross-sections in each ping. We must then determine if the geometric centre of the cross-section approximates the geometric centre of the target (a tricky task, as we have discussed), in order to determine whether we should then track the target across multiple pings or whether we should scan through it. We have shown that this relates to the size of the target in relation to the sampling volume, along with what else we might confidently know about the insonified targets. In Echoview, the Multibeam Target Detection operator is designed specifically to detect point-target cross-sections, with the next step being to track them with the fish tracking algorithm. For extended targets, the cross-sections are not detected with the Multibeam Target Detection operator, even though the approach is conceptually identical, but as part of the 3D schools detection algorithm (whether by ping or cruise scanning).

4.6. Future directions for deep-sea water-column echosounding

This study demonstrates the importance of close collaboration between hardware and software engineers, acousticians and aquatic ecologists. There were a number of limitations inherent in the survey design that could be improved in future echosounder surveys of the BBL. Range biases in the data could be addressed by repeating each transect at a number of different altitudes. The reduction of vessel avoidance might be achieved by orienting the MBES horizontally, on

the assumption that radiated noise and any other stimuli are weaker out to the side of the AUV (see e.g. Benoit-Bird and Au, 2009). The limitations inherent in the SeaBat 7125 system (especially sidelobe interference and the marginal sampling resolution relative to the size of the targets) could be addressed by leveraging the strengths of other types of echosounder system, notwithstanding the practical considerations regarding installation on a deep-deployed AUV. For example: imaging sonars (ultra-high-resolution swath MBES systems) have a higher sampling resolution (e.g. Kupilik and Petersen, 2014); wideband (aka broadband) SBES systems are capable of higher-resolution target detection (using match-filtering techniques, aka pulse compression; e.g. Stanton et al., 2010), greater discrimination of targets close to the seafloor (through pulse-ramping techniques; e.g. Lavery et al., 2017) and wideband species identification (e.g. Ross et al., 2013; Jech et al., 2017) out to considerable range; split-beam MBES systems facilitate calibration (e.g. Trenkel et al., 2008; Melvin and Cochrane, 2014); MBES systems that vary the frequency between beams have reduced sidelobes (e.g. Andersen et al., 2006); and omnidirectional and 3D MBES systems sample a greater volume of water (e.g. Andersen et al., 2006; Vatnehol, 2016; Matte et al., 2017). In addition, the interpretation of the echosounder data will be improved by deploying complementary monitoring technologies (trawls, HOVs, ROVs, cameras, landers) in close spatial and temporal proximity to the survey.

5. Conclusions

The results demonstrate that an AUV-mounted MBES has the potential to provide unique and detailed information on the *in situ* abundance, distribution, size and behaviour of deep-sea benthopelagic animals. This remote-sensing approach addresses some of the limitations of existing deep-sea monitoring technologies in that it is considerably less invasive and can rapidly sample significant volumes of water at relatively high spatial and temporal resolution. However, the inherent limitations of the echosounder data and the potential for vessel avoidance must be considered. We provide detailed data-processing information for those interested in working with water-column MBES data, a critical appraisal of the data in the context of aquatic ecosystem research, and a consideration of future directions for deep-sea water-column echosounding.

Acknowledgements

We gratefully acknowledge: the crew of the RV Rachel Carson for assistance in the field; Briony Hutton (Echoview Software), Ben Scoulding (CSIRO) and Geoff Matt (Echoview Software) for valuable discussions regarding MBES data formats and data processing, and for comments on a draft of the paper; Gorm Wendelboe (RESON) for clarification on SeaBat 7125 sample backscatter measurements; Dave Demer (NOAA) for technical assistance with MBES backscattering terms, units and equations; and Linda Kuhnz (MBARI) for providing information, images and footage of the benthopelagic fauna at the MARS observatory.

References

Andersen, L.N., Berg, S., Gammelsaeter, O.B., Lunde, E.B., 2006. New scientific multi-beam systems (ME70 and MS70) for fishery research applications. J. Acoust. Soc. Am. 120. http://dx.doi.org/10.1121/1.4787077. (3017-3017).

Anderson, M.E., 1980. Aspects of the natural history of the midwater fish *Lycodapus mandibularis* (Zoarcidae) in Monterey Bay, California. Pac. Sci. 34, 181–194. http://dx.doi.org/hdl.handle.net/10125/1618.

Angel, M.V., Boxshall, G.A., 1990. Life in the benthic boundary layer: connections to the mid-water and sea floor. Philos. Trans. R. Soc. A 331, 15–28. http://dx.doi.org/10. 1098/rsta.1990.0053.

Axelsen, B.E., Anker-Nilssen, T., Fossum, P., Kvamme, C., Nøttestad, L., 2001. Pretty patterns but a simple strategy: predator-prey interactions between juvenile herring and Atlantic puffins observed with multibeam sonar. Can. J. Zool. 79, 1586–1596. http://dx.doi.org/10.1139/z01-113.

Bailey, D.M., Genard, B., Collins, M.A., Rees, J.F., Unsworth, S.K., Battle, E.J., Bagley,

- P.M., Jamieson, A.J., Priede, I.G., 2005. High swimming and metabolic activity in the deep-sea eel *Synaphobranchus kaupii* revealed by integrated *in situ* and *in vitro* measurements. Physiol. Biochem. Zool. 78, 335–346. http://dx.doi.org/10.1086/430042.
- Benoit-Bird, K.J., Au, W.L., 2009. Cooperative prey herding by the pelagic dolphin, Stenella longirostris. J. Acoust. Soc. Am. 125, 125–137. http://dx.doi.org/10.1121/1
- Benoit-Bird, K.J., Lawson, G.L., 2016. Ecological insights from pelagic habitats acquired using active acoustic techniques. Annu. Rev. Mar. Sci. 8, 463–490. http://dx.doi.org/ 10.1146/annurey-marine-122414-034001.
- 10.1146/annurev-marine-122414-034001.

 Benoit-Bird, K.J., Moline, M.A., Southall, B.L., 2017. Prey in oceanic sound scattering layers organize to get a little help from their friends. Limnol. Oceanogr. 62, 2788–2798. http://dx.doi.org/10.1002/lno.10606.
- Bertrand, A., Josse, E., Bach, P., Dagorn, L., 2003. Acoustics for ecosystem research: lessons and perspectives from a scientific programme focusing on tuna-environment relationships. Aquat. Living Res. 16, 197–203. http://dx.doi.org/10.1016/S0990-7440(03)00018-4.
- Blackman, S.S., 1986. Multiple-Target Tracking With Radar Applications. Artech House Publishers Inc, Dedham, MA, USA.

 Brown, C.J., Blondel, P., 2009. Developments in the application of multibeam sonar
- frown, C.J., Blondel, P., 2009. Developments in the application of multibeam sonar backscatter for seafloor habitat mapping. Appl. Acoust. 70, 1242–1247. http://dx. doi.org/10.1016/j.apacoust.2008.08.004.
- Buelens, B., Williams, R., Sale, A.H.J., Pauly, T., 2006. Computational challenges in processing and analysis of full-watercolumn multibeam sonar data. in: Proceedings of the Eighth European Conference on Underwater Acoustics. 12-15 June, Carvoeiro, Portugal.
- Cailliet, G.M., Andrews, A.H., Wakefield, W.W., Moreno, G., Rhodes, K.L., 1999. Fish faunal and habitat analyses using trawls, camera sleds and submersibles in benthic deep-sea habitats off central California. Oceanol. Acta 22, 579–592. http://dx.doi.org/10.1016/S0399-1784(00)88949-5.
- Caress, D.W., Thomas, H., Kirkwood, W.J., McEwen, R., Henthorn, R., Clague, D.A., Paull,
 C.K., Paduan, J., Maier, K.L., 2008. High-resolution multibeam, sidescan, and subbottom surveys using the MBARI AUV D. Allan B. In: Greene, H.G., Reynolds, J.R. (Eds.), Marine Habitat Mapping Technology for Alaska. Alaska Sea Grant College Program, University of Alaska, Fairbanks, pp. 47–69.
 Clarke, M.E., Whitmire, C., Fruh, E., Anderson, J., Taylor, J., Rooney, J., Ferguson, S.,
- Clarke, M.E., Whitmire, C., Fruh, E., Anderson, J., Taylor, J., Rooney, J., Ferguson, S., Singh, H., 2010. Developing the SeaBED AUV as a tool for conducting routine surveys of fish and their habitat in the Pacific. in: Proceedings of 2010 IEEE/OES Autonomous Underwater Vehicles (AUV). 1-3 September, Monterey, USA, http://dx.doi.org/10. 1109/AUV.2010.5779665.
- Colbo, K., Ross, T., Brown, C., Weber, T., 2014. A review of oceanographic applications of water column data from multibeam echosounders. Estuar. Coast. Shelf S. 145, 41–56. http://dx.doi.org/10.1016/j.ecss.2014.04.002.
- Collins, M.A., Bailey, D.M., Ruxton, G.D., Priede, I.G., 2005. Trends in body size across an environmental gradient: a differential response in scavenging and non-scavenging demersal deep-sea fish. Philos. Trans. R. Soc. B 272, 2051–2057. http://dx.doi.org/ 10.1098/rspb.2005.3189.
- Cox, M.J., Demer, D.A., Warren, J.D., Cutter, G.R., Brierley, A.S., 2009. Multibeam echosounder observations reveal interactions between Antarctic krill and airbreathing predators. Mar. Ecol. Prog. Ser. 378, 199–209. http://dx.doi.org/10.3354/ peps/1795
- Cutter, G.R., Demer, D.A., 2007. Accounting for scattering directivity and fish behaviour in multibeam-echosounder surveys. ICES J. Mar. Sci. 64, 1664–1674. http://dx.doi. org/10.1093/icesjms/fsm151.
- Cutter, G.R., Renfree, J.S., Cox, M.J., Brierley, A.S., Demer, D.A., 2009. Modelling three-dimensional directivity of sound scattering by Antarctic krill: progress towards biomass estimation using multibeam sonar. ICES J. Mar. Sci. 66, 1245–1251. http://dx.doi.org/10.1093/icesjms/fsp040.
- Danovaro, R., Snelgrove, P.V., Tyler, P., 2014. Challenging the paradigms of deep-sea ecology. Trends Ecol. Evol. 29, 465–475. http://dx.doi.org/10.1016/j.tree.2014.06.
- De Robertis, A., Handegard, N.O., 2012. Fish avoidance of research vessels and the efficacy of noise-reduced vessels: a review. ICES J. Mar. Sci. 70, 34–35. http://dx.doi. org/10.1093/icesims/fss155.
- Demer, D.A., Berger, L., Bernasconi, M., Bethke, E., Boswell, K., Chu, D., Domokos, R., et al. 2015. Calibration of acoustic instruments. ICES Cooperative Research Report No. 326, 130pp.
- Dickey, T.D., Itsweire, E.C., Moline, M.A., Perry, M.J., 2008. Introduction to the Limnology and Oceanography special issue on autonomous and Lagrangian platforms and sensors (ALPS). Limnol. Oceanogr. 53, 2057–2061. http://dx.doi.org/10.4319/ lo.2008.53.5 part 2.2057.
- Drazen, J.C., Seibel, B.A., 2007. Depth-related trends in metabolism of benthic and benthopelagic deep-sea fishes. Limnol. Oceanogr. 52, 2306–2316. http://dx.doi.org/ 10.4319/lo.2007.52.5.2306.
- Echoview Software, 2016. Echoview Help file 7.1.12 for Echoview 7.1.24. http://support.echoview.com/WebHelp/Echoview.htm (21st Sep 2016). (Last accessed Jan 2017). Eittreim, S.L., Embley, R.W., Normark, W.R., Greene, H.G., McHugh, C.M., Ryan, W.B.F.,
- Eittreim, S.L., Embley, R.W., Normark, W.R., Greene, H.G., McHugh, C.M., Ryan, W.B.F., 1989. Observations in Monterey Canyon and fan valley using the submersible Alvin and a photographic sled. US Geol. Surv. 89–291 (Open-File Report).
- Fernandes, P.G., Stevenson, P., Brierley, A.S., Armstrong, F., Simmonds, E.J., 2003. Autonomous underwater vehicles: future platforms for fisheries acoustics. ICES J. Mar. Sci. 60, 684–691. http://dx.doi.org/10.1016/S1054-3139(03)00038-9.
- Fernandes, P.G., Copland, P., Garcia, R., Nicosevici, T., Scoulding, B., 2016. Additional evidence for fisheries acoustics: small cameras and angling gear provide tilt angle distributions and other relevant data for mackerel surveys. ICES J. Mar. Sci. 73, 2009–2019. http://dx.doi.org/10.1093/icesjms/fsw091.
- Foote, K.G., 1983. Linearity of fisheries acoustics, with addition theorems. J. Acoust. Soc. Am. 73, 1932–1940. http://dx.doi.org/10.1121/1.389583.
- Foote, K.G., Chu, D., Hammar, T.R., Baldwin, K.C., Mayer, L.A., Hufnagle Jr, L.C., Jech, J.M., 2005. Protocols for calibrating multibeam sonar. J. Acoust. Soc. Am. 117, 2013–2027. http://dx.doi.org/10.1121/1.1869073.

- Gage, J.D., Tyler, P.A., 1991. Deep-Sea Biology: A Natural History of Organisms at the Deep-Sea Floor. Cambridge University Press.
- Deep-Sea Floor. Cambridge University Press.

 Galparsoro, I., Rodríguez, J.G., Menchaca, I., Quincoces, I., Garmendia, J.M., Borja, Á., 2015. Benthic habitat mapping on the Basque continental shelf (SE Bay of Biscay) and its application to the European Marine Strategy Framework Directive. J. Sea Res. 100, 70–76. http://dx.doi.org/10.1016/j.seares.2014.09.013.
- Gee, L., Doucet, M., Parker, D., Weber, T., Beaudoin, J., 2012. Is Multibeam Water Column Data Really Worth the Disk Space? Hydro12 Conference Proceedings. 13–15 November. Rotterdam.
- Gerlotto, F., Soria, M., Fréon, P., 1999. From two dimensions to three: the use of multibeam sonar for a new approach in fisheries acoustics. Can. J. Fish. Aquat. Sci. 56, 6–12. http://dx.doi.org/10.1139/f98-138.
- Griffiths, G., Enoch, P., Millard, N.W., 2001. On the radiated noise of the Autosub autonomous underwater vehicle. ICES J. Mar. Sci. 58, 1195–1200. http://dx.doi.org/10.1006/jmsc.2001.1120.
- Greenaway, S.F., Weber, T.C., 2010. Test methodology for evaluation of linearity of multibeam echosounder backscatter performance. In: OCEANS 2010 MTS/IEEE, Sydney, Australia, pp. 1–7. http://dx.doi.org/10.1109/OCEANS.2010.5664383.
 Guihen, D., Fielding, S., Murphy, E.J., Heywood, K.J., Griffiths, G., 2014. An assessment
- Guihen, D., Fielding, S., Murphy, E.J., Heywood, K.J., Griffiths, G., 2014. An assessment of the use of ocean gliders to undertake acoustic measurements of zooplankton: the distribution and density of Antarctic krill (*Euphausia superba*) in the Weddell Sea. Limnol. Oceanogr. 12, 373–389. http://dx.doi.org/10.4319/lom.2014.12.373. Herring, P., 2001. The Biology of the Deep Ocean. OUP, Oxford.
- Hightower, J.E., Magowan, K.J., Brown, L.M., Fox, D.A., 2013. Reliability of fish size estimates obtained from multibeam imaging sonar. J. Fish. Wild Manag. 4, 86–96. http://dx.doi.org/10.3996/102011-JFWM-061.
- Hughes Clarke, J.E., Lamplugh, M., Czotter, K., 2006. Multibeam water column imaging: improved wreck least-depth determination. Canadian Hydrographic Conference, May 2006, Halifax, Canada.
- Jackson, D.R., Richardson, M.D., 2007. High-frequency Seafloor Acoustics. Springer, New York.
- Jacobsen Stout, N., Kuhnz, L., Lundsten, L., Schlining, B., Schlining K., von Thun, S., (eds.). 2016 The Deep-Sea Guide (DSG). Monterey Bay Aquarium Research Institute (MBARI). Consulted on: 2016-10-20.
- Jech, J.M., Lawson, G.L., Lavery, A.C., 2017. Wideband (15–260 kHz) acoustic volume backscattering spectra of Northern krill (*Meganyctiphanes norvegica*) and butterfish (*Peprilus triacanthus*). ICES J. Mar. Sci. 74, 2249–2261. https://doi.org/10.1093/ icesjms/fsx050.
- Jones, E.G., Tselepides, A., Bagley, P.M., Collins, M.A., Priede, I.G., 2003. Bathymetric distribution of some benthic and benthopelagic species attracted to baited cameras and traps in the deep eastern Mediterranean. Mar. Ecol. Prog. Ser. 251, 75–86. http:// dx.doi.org/10.3354/meps251075.
- Kieser, R., Mulligan, T.J., 1984. Analysis of echo counting data: a model. Can. J. Fish. Aquat. Sci. 41, 451–458. http://dx.doi.org/10.1139/f84-054.
- Kloser, R.J., 1996. Improved precision of acoustic surveys of benthopelagic fish by means of a deep-towed transducer. ICES J. Mar. Sci. 53, 407–413. http://dx.doi.org/10. 1006/imsc.1996.0057.
- Korneliussen, R.J., Diner, N., Ona, E., Berger, L., Fernandes, P.G., 2008. Proposals for the collection of multifrequency acoustic data. ICES J. Mar. Sci. 65, 982–994. http://dx. doi.org/10.1093/icesjms/fsn052.
- Koslow, J., Boehlert, G.W., Gordon, J.D.M., Haedrich, R.L., Lorance, P., Parin, N., 2000. Continental slope and deep-sea fisheries: implications for a fragile ecosystem. ICES J. Mar. Sci. 57, 548–557. http://dx.doi.org/10.1006/jmsc.2000.0722.
- Kovesi, P., 1999. Phase preserving denoising of images. In: Australian Pattern Recognition. Society Conference. Digital Image Computing: Techniques and Applications. Perth, Australia, pp. 212–217.
- Kupilik, M., Petersen, T., 2014. Imaging sonar tracking of salmon for size and tail beat frequency. IEEE Signal and Information Processing (GlobalSIP), Atlanta, Georgia, USA, pp. 1127–1131.
- Lanzoni, J.C., Weber, T.C., 2011. A method for field calibration of a multibeam echo sounder. OCEANS'11 MTS/IEEE KONA, Hawaii, USA, pp. 1–7.
- Lavery, A.C., Bassett, C., Lawson, G.L., Jech, J.M., 2017. Exploiting signal processing approaches for broadband echosounders. ICES J. Mar. Sci. 74, 2262–2275. https://doi.org/10.1093/icesjms/fsx155.
- Lurton, X., 2002. An Introduction to Underwater Acoustics: Principles and Applications. Springer Science & Business Media, Praxis Publishing Ltd, Chichester, UK.
- MacLennan, D.N., Fernandes, P.G., Dalen, J., 2002. A consistent approach to definitions and symbols in fisheries acoustics. ICES J. Mar. Sci. 59, 365–369. http://dx.doi.org/ 10.1006/jmsc.2001.1158.
- MacNeil, M.A., McMeans, B.C., Hussey, N.E., Vecsei, P., Svavarsson, J., Kovacs, K.M., Lydersen, C., Treble, M.A., Skomal, G.B., Ramsey, M., Fisk, A.T., 2012. Biology of the Greenland shark Somniosus microcephalus. J. Fish. Biol. 80, 991–1018. http://dx.doi.org/10.1111/j.1095-8649.2012.03257.x.
- Malzone, C., Lockhart, D., Meurling, T., Baldwin, M., 2008. The progression and impact of the latest generation of multibeam acoustics upon multidisciplinary hydrographicbased applications. Underw. Technol. 27, 151–160. http://dx.doi.org/10.1111/j. 1095-8649.2012.03257.x.
- Mann, D.A., Hawkins, A.D., Jech, J.M., 2008. Active and passive acoustics to locate and study fish. In: Webb, J.F., Fay, R.R., Popper, A.N. (Eds.), Fish Bioacoustics. Springer, New York, pp. 279–309.
- Matte, G., Charlot, D., Lerda, O., N'Guyen, T.K., Giovanni, V., Rioblanc, M., Mosca, F., 2017. SeapiX: an innovative multibeam multiswath echosounder for water column and seabed analysis. In: Hydro17 Conference Proceedings. 21–23 December, Rotterdam.
- McCave, I.N., 1976. The Benthic Boundary Layer. Plenum Press, New York, USA.
- Melvin, G.D., Cochrane, N.A., Li, Y., 2003. Extraction and comparison of acoustic back-scatter from a calibrated multi-and single-beam sonar. ICES J. Mar. Sci. 60, 669–677. http://dx.doi.org/10.1016/S1054-3139(03)00055-9.
- Melvin, G.D., Cochrane, N.A., 2014. Multibeam acoustic detection of fish and water column targets at high-flow sites. Estuar. Coast. 38, 227–240. http://dx.doi.org/10.

- 1016/S1054-3139(03)00055-9.
- Moline, M.A., Benoit-Bird, K., O'Gorman, D., Robbins, I.C., 2015. Integration of scientific echo sounders with an adaptable autonomous vehicle to extend our understanding of animals from the surface to the bathypelagic. J. Atmos. Ocean. Technol. 32, 2173–2186. http://dx.doi.org/10.1175/JTECH-D-15-0035.1.
- Moline, M.A., Benoit-Bird, K., 2016. Sensor fusion and autonomy as a powerful combination for biological assessment in the marine environment. Robotics 5, 4. http://dx.doi.org/10.3390/robotics5010004.
- Ona, E., 1999. Methodology for target strength measurements. ICES Coop. Res. Report. 235, 59.
- Patel, R., Handegard, N.O., Godø, O.R., 2004. Behaviour of herring (*Clupea harengus* L.) towards an approaching autonomous underwater vehicle. ICES J. Mar. Sci. 61, 1044–1049. http://dx.doi.org/10.1016/j.icesjms.2004.07.002.
- Peña, M., 2016. Incrementing data quality of multi-frequency echograms using the Adaptive Wiener Filter (AWF) denoising algorithm. Deep Sea Res. I. 116, 14–21. http://dx.doi.org/10.1016/j.dsr.2016.07.008.
- http://dx.doi.org/10.1016/j.dsr.2016.07.008.

 Raymond, E.H., 2008. Unobtrusive Observations in the Deep Sea (Ph.D. thesis). The Johns Hopkins University.
- Renard, V., Allenou, J.P., 1979. Sea beam, multi-beam echo-sounding in "Jean Charcot": Description, evaluation and first results. Int. Hydrogr. Rev. 56, 35–67.
- RESON, 2011. SeaBat 7125 SV2 High-Resolution Multibeam Sonar System, Operator's Manual. Version 3, July 2011.
- RESON, 2016. Data Format Definition Document, 7k Data Format, Volume 1. Version 2. 44. June 2016.
- Robison, B.H., 2004. Deep pelagic biology. J. Exp. Mar. Biol. Ecol. 300, 253–272. http://dx.doi.org/10.1016/j.jembe.2004.01.012.
- Ross, T., Keister, J.E., Lara-Lopez, A., 2013. On the use of high-frequency broadband sonar to classify biological scattering layers from a cabled observatory in Saanich Inlet, British Columbia. Method. Oceanogr. 5, 19–38. http://dx.doi.org/10.1016/j. pio. 2013.05.001.
- Rudstam, L.G., Jech, J.M., Parker-Stetter, S.L., Horne, J.K., Sullivan, P.J., Mason, D.M., 2012. Fisheries Acoustics. Fisheries Techniques, 3rd ed. American Fisheries Society, Bethesda, pp. 597–636.
- Simmonds, J.E., MacLennan, D.N., 2005. Fisheries Acoustics: Theory and Practice, 2nd ed. Blackwell Science Ltd, Oxford, UK.
- Simmons, S.M., Parsons, D.R., Best, J.L., Orfeo, O., Lane, S.N., Kostaschuk, R., Hardy, R.J., West, G., Malzone, C., Marcus, J., Pocwiardowski, P., 2009. Monitoring suspended sediment dynamics using MBES. J. Hydraul. Eng. 136, 45–49. http://dx.doi.org/10. 1061/??ASCE??HY.1943-7900.0000110.
- Smith Jr, K.L., 1982. Zooplankton of a bathyal benthic boundary layer: In situ rates of oxygen consumption and ammonium excretion. Limnol. Oceanogr. 27, 461–471. http://dx.doi.org/10.4319/lo.1982.27.3.0461.
- Smith Jr, K.L., Alexandrou, D., Edelman, J.L., 1989. Acoustic detection and tracking of abyssopelagic animals: description of an autonomous split-beam acoustic array. Deep Sea Res. 36, 1427–1441. http://dx.doi.org/10.1016/0198-0149(89)90093-9.
- Smith Jr, K.L., 1992. Benthic boundary layer communities and carbon cycling at abyssal depths in the central North Pacific. Limnol. Oceanogr. 37, 1034–1056. https://doi. org/10.4319/lo.1992.37.5.103.
- Smith Jr, K.L., Kaufmann, R.S., Edelman, J.L., Baldwin, R.J., 1992. Abyssopelagic fauna in the central North Pacific: comparison of acoustic detection and trawl and baited trap collections to 5800 m. Deep Sea Res. 39, 659–685. http://dx.doi.org/10.1016/ 0198-0149(92)90094-A.
- Smith Jr, K.L., Baldwin, R.J., 1997. 9 Laboratory and *in situ* methods for studying deep-Sea fishes. Fish. Phys. 16, 351–378. https://doi.org/10.1016/S1546-5098(08)
- Smith Jr, K.L., Ruhl, H.A., Bett, B.J., Billett, D.S.M., Lampitt, R.S., Kaufmann, R.S., 2009. Climate, carbon cycling, and deep-ocean ecosystems. Proc. Natl. Acad. Sci. USA 106, 19211–19218. https://doi.org/10.1073/pnas.0908322106.

- Spampinato, C., Giordano, D., Di Salvo, R., Chen-Burger, Y.H.J., Fisher, R.B., Nadarajan, G., 2010. Automatic fish classification for underwater species behavior understanding. In: Proceedings of the first ACM international workshop on Analysis and retrieval of tracked events and motion in imagery streams, October 2010, Firenze, Italy, pp. 45–50.
- Stanton, T.K., Chu, D., Jech, J.M., Irish, J.D., 2010. New broadband methods for resonance classification and high-resolution imagery of fish with swimbladders using a modified commercial broadband echosounder. ICES J. Mar. Sci. 67, 365–378. http://dx.doi.org/10.1093/icesjms/fsp262.
- Stefanescu, C., Rucabado, J., Lloris, D., 1992. Depth-size trends in western Mediterranean demersal deep-sea fishes. Mar. Ecol. Prog. Ser. 81, 205–213. http://dx.doi.org/10. 3354/meps081205.
- Stoner, A.W., Ryer, C.H., Parker, S.J., Auster, P.J., Wakefield, W.W., 2008. Evaluating the role of fish behavior in surveys conducted with underwater vehicles. Can. J. Fish. Aquat. Sci. 65, 1230–1243. http://dx.doi.org/10.1139/F08-032.
- Tolimieri, N., Clarke, M.E., Singh, H., Goldfinger, C., 2008. Evaluating the SeaBED AUV for Monitoring Groundfish in Untrawlable Habitat. Marine Habitat Mapping Technology for Alaska. Alaska Sea Grant College Program, University of Alaska Fairbanks, Fairbanks, AK, pp. 129–141.
- Trenkel, V.M., Mazauric, V., Berger, L., 2008. The new fisheries multibeam echosounder ME70: description and expected contribution to fisheries research. ICES J. Mar. Sci. 65, 645–655. http://dx.doi.org/10.1093/icesjms/fsn051.
- Trenkel, V.M., Berger, L., 2013. A fisheries acoustic multi-frequency indicator to inform on large scale spatial patterns of aquatic pelagic ecosystems. Ecol. Indic. 30, 72–79. http://dx.doi.org/10.1016/j.ecolind.2013.02.006.
- Urmy, S.S., Horne, J.K., Barbee, D.H., 2012. Measuring the vertical distributional variability of pelagic fauna in Monterey Bay. ICES J. Mar. Sci. 69, 184–196. http://dx.doi.org/10.1093/icesjms/fsr205.
- Vatnehol, S., 2016. Increasing the Biomass Estimation Accuracy of a Single Fish School Using a Cylindrical Multi-beam Fishery Sonar (Ph.D. thesis). University of Bergen. http://dspace.uib.no/bitstream/handle/1956/13136/dr-thesis-2016-Sindre-Vatnehol.pdf.
- Webb, T.J., Berghe, E.V., O'Dor, R., 2010. Biodiversity's big wet secret: the global distribution of marine biological records reveals chronic under-exploration of the deep pelagic ocean. PLoS One 5, e10223. http://dx.doi.org/10.1371/journal.pone.0010223.
- Weber, T.C., Peña, H., Jech, J.M., 2009. Consecutive acoustic observations of an Atlantic herring school in the Northwest Atlantic. ICES J. Mar. Sci. 66, 1270–1277. http://dx.doi.org/10.1093/icesjms/fsp090.
- Weber, T., Mayer, L.A., Beaudoin, J., Jerram, K., Malik, M.A., Shedd, B., Rice, G., 2012. Mapping gas seeps with the deepwater multibeam echosounder on *Okeanos Explorer*. Oceanography 25, 54–55. http://dx.doi.org/10.5670/oceanog.2011.supplement.01.
- Welton, B., 2014. A Field Method for Backscatter Calibration Applied to NOAA's Reson 7125 Multibeam Echo-Sounders (Ph.D. thesis). University of New Hampshire.
- Wendelboe, G., Dahl, H., Maillard, E., Bjørnø, L., 2012. Towards a fully calibrated multibeam echosounder. In: Proceedings of Meetings on Acoustics 17, 070025. http://dx.doi.org/10.1121/14767979
- Widder, E.A., Robison, B.H., Reisenbichler, K.R., Haddock, S.H.D., 2005. Using red light for in situ observations of deep-sea fishes. Deep Sea Res. 52, 2077–2085. http://dx. doi.org/10.1016/j.dsr.2005.06.007.
- Wiebe, P.H., Copley, N., Van Dover, C., Tamse, A., Manrique, F., 1988. Deep-water zooplankton of the Guaymas basin hydrothermal vent field. Deep Sea Res. 35, 985–1013. http://dx.doi.org/10.1016/0198-0149(88)90072-6.
- Wishner, K.F., 1980. The biomass of the deep-sea benthopelagic plankton. Deep Sea Res. 27, 203–216. http://dx.doi.org/10.1016/0198-0149(80)90012-6.
- Yeh, J., Drazen, J.C., 2011. Baited-camera observations of deep-sea megafaunal scavenger ecology on the California slope. Mar. Ecol. Prog. Ser. 424, 145–156. http://dx.doi. org/10.3354/meps08972.